

Overview No. 142

## Indentation across size scales and disciplines: Recent developments in experimentation and modeling

Andrew Gouldstone<sup>a,\*</sup>, Nuwong Chollacoop<sup>b</sup>, Ming Dao<sup>c</sup>, Ju Li<sup>d</sup>,  
Andrew M. Minor<sup>e</sup>, Yu-Lin Shen<sup>f</sup>

<sup>a</sup> Department of Materials Science and Engineering, SUNY Stony Brook, Heavy Engineering 130, Stony Brook, NY 11974, USA

<sup>b</sup> National Metal and Materials Technology Center (MTEC), 114 Paholyothin Road, Pathumthani 12120, Thailand

<sup>c</sup> Department of Materials Science and Engineering, Massachusetts Institute of Technology, Cambridge, MA 02139, USA

<sup>d</sup> Department of Materials Science and Engineering, The Ohio State University, Columbus, OH 43210, USA

<sup>e</sup> National Center for Electron Microscopy, Lawrence Berkeley National Laboratory, Berkeley, CA 94720, USA

<sup>f</sup> Department of Mechanical Engineering, University of New Mexico, Albuquerque, NM 87131, USA

Received 9 June 2006; received in revised form 23 August 2006; accepted 28 August 2006

Available online 16 November 2006

### Abstract

Indentation is a remarkably flexible mechanical test due to its relative experimental simplicity. Coupled with advances in instrument development, ease of implementation has made indentation a ubiquitous research tool for a number of different systems across size scales (nano to macro) and scientific/engineering disciplines. However, the exploration of different materials systems and the potential usage of indentation as a precise and quantitative method beyond the research laboratory have prompted intense modeling and interpretation efforts for robust analysis of experimental results. In this review, we describe progress in a number of different aspects of this method, including continuum-based modeling of homogeneous and heterogeneous systems, microstructural size effects and atomic modeling of nanoindentation experiments, in situ transmission electron microscopy observations of nanoscale contact, and novel and emerging uses for indentation. A recurring theme is the consideration of what is meant by “hardness” in different physical scenarios.

© 2006 Acta Materialia Inc. Published by Elsevier Ltd. All rights reserved.

**Keywords:** Microindentation; Nanoindentation; Transmission electron microscopy (TEM); Finite element analysis; Simulation

### 1. Introduction

For over a century, indentation has been employed to probe the mechanical behavior of materials for a wide range of engineering applications. The main reason for its ubiquitous use is its intrinsic experimental simplicity; indentation requires minimal specimen preparation and/or mounting, can be performed several times on a single specimen, and can probe different volumes of materials via appropriate choice of load and tip geometry. In addition, aggressive instrument development has made possible the application of forces from kilo-newtons down to pico-

newtons, and local displacements down to nanometers; virtually any solid can be indented, including bulk materials, biological entities and nanostructures. However, the strain fields under an indenter are complex and even for bulk isotropic materials, analysis of data is non-trivial. For more complicated materials systems (e.g. thin films, small volumes, porous structures, biomaterials), indentation response is tied to specific aspects of material behavior yet effective interpretation requires expertise in both indentation mechanics and the physics of the system being indented.

This challenge, along with the ever-increasing availability of commercial indenter systems, has driven a major increase in indentation as a research tool. However, in contrast to other established mechanical tests, e.g. uniaxial

\* Corresponding author. Tel.: +1 631 632 4701; fax: +1 631 632 7878.

E-mail address: [bubbleraft@gmail.com](mailto:bubbleraft@gmail.com) (A. Gouldstone).

tension, the goal of indentation experiments is not always to extract a “value”, or rather, should not be. As has been noted in the literature, and will be shown in this review, the concepts of hardness and modulus, as extracted via indentation, are manufactured parameters that are strongly dependent upon tip geometry, elastic and inelastic material behavior, and specimen boundary conditions. That this is beginning to be recognized in scientific circles is partially illustrated by the increasing use of the term “indentation modulus” when reporting results, and careful scrutiny in comparison of indentation-extracted properties to those under different loading conditions. Indeed, as more complex material systems are probed via indentation, robust scientific conclusions can only be strengthened by maintaining this perspective.

This review addresses the implementation and interpretation of indentation in a number of different scenarios of current and emerging importance. We begin with state-of-the-art analyses of indentation results (load–depth, or  $P$ – $h$  curves) from a purely continuum perspective, for bulk materials. As indentation is heavily used in multilayered or heterogeneous material systems, a review of (continuum-based) analyses of such systems follows. Appropriately, we then address observations and interpretation of the indentation size effect, in bulk metallic materials and other systems, to bridge the gap between continuum approaches and consideration of discrete dislocation events under ultra-low loads, via direct observation and atomic modeling. Finally, we describe a number of non-traditional uses of indentation in other fields, to shed light on mechanical behavior, nanostructure or even physiology of different materials.

## 2. Extracting mechanical properties of bulk materials with instrumented indentation

### 2.1. Indenter tips, hardness of metals, and instrumented indentation

Fig. 1 shows three types of indenter tips commonly used in experiments and/or analyses. Sharp (Fig. 1(a)) and spherical (Fig. 1(b)) indenters are, to a first order, suited for different types of experiments. For example, the self-similarity of a sharp tip makes it more favorable for analysis of ductile materials, simplifying the extraction of elastic–plastic properties. Conversely, the spherical tip has been more widely used for brittle materials, or more complex systems in which a small-strain elastic deformation is preferable for simpler analysis, but yet has been used in extracting elastic–plastic properties as well. On the micro- or nanoscale, the finite (albeit small) tip radius on a real sharp tip cannot be neglected (Fig. 1(c)) and thus knowledge of tip characteristics either via direct measurement or indirect calibration of an area function is critical for accurate analysis. As this review contains descriptions across materials and size scales, tip characteristics will be explicitly stated for clarity. In the following section, we

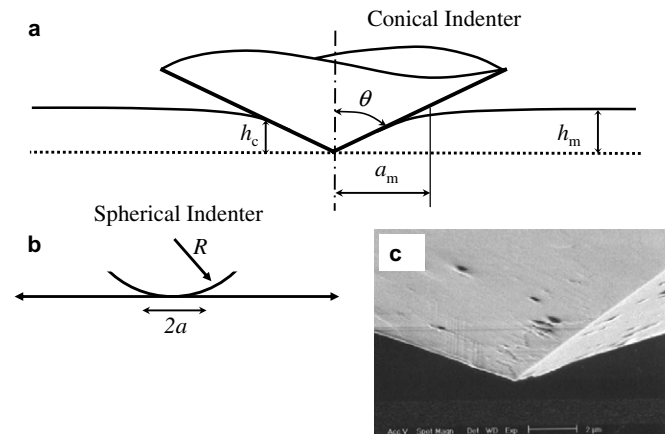


Fig. 1. Schematic of tips used in instrumented indentation. (a) A sharp pyramidal tip is often modeled as a cone with  $\alpha = 70.3^\circ$ . (b) A spherical tip is defined by its radius  $R$ , and a characteristic strain may be defined as  $a/R$ . Stress fields under elastic loading are well defined in closed form. (c) SEM image of a diamond Berkovich indenter with blunt tip radius  $R \approx 50$  nm [102].

focus primarily on sharp indentation of ductile metals. (For a discussion of spherical indentation the reader is referred to Refs. [1–6].)

The “hardness” of a metal has, for a long time, been a convenient descriptor of its resistance to plastic deformation. Hardness measurements are simple: a load  $P$  is applied to a flat surface with a rigid pyramidal tip, and the resulting imprint area  $A$  measured. Early researchers proposed that the hardness  $H = P/A$  has the following relationship [7]

$$H = 3\sigma_{0.08}, \quad (1)$$

where  $\sigma_{0.08}$  is the compressive flow stress of the tested metal, at a representative strain of approximately 8%. Eq. (1) has been widely used in the materials community for more than half a century, and its accuracy and applicable range have been carefully studied and re-examined in the past 10 years or so [8,9]. It is inspiring and slightly humbling to mention that these and other contact mechanics analyses prior to the 1970s were performed without the aid of computers.

One factor that has limited the applicability of hardness tests on smaller scales is the need to accurately measure imprint dimensions (contact area) after unloading. However, recent technological advances in instrumentation, and especially computational power, have led to significant expansion in indentation interpretation. Depth-sensing indentation can now be used to accurately extract not only hardness, but the entire compressive stress–strain curve of bulk metals [9–16], including elastic modulus, plastic stress–strain behavior and creep directly from the load ( $P$ ) vs. penetration depth ( $h$ ) curve, without the need for measuring residual contact impression [8,14–16]. In addition, various methodologies have also been developed to extract elastically graded properties from spherical indentation [17–23], evaluate residual stresses from sharp indentation

[24–28], extract elastic–plastic stress–strain behavior from spherical indentation [2–6], compute electrical–mechanical coupled properties from indentation of piezoelectric solids [29–33], measure power law creep parameters [34–36], and evaluate viscoelastic properties [9,36].

Fig. 2 shows the typical indentation response ( $P$ – $h$  curve) of a homogeneous elastic–plastic material by a sharp indenter tip (Fig. 1(a)), with salient features described here. The loading curve is considered to follow Kick’s law,  $P = Ch^2$ , where  $C$  depends on elastic and plastic material properties, as well as indenter geometry. At maximum depth,  $h_m$ , or maximum load,  $P_m$ , the average contact pressure,  $p_{ave} = P_m/A_m$  ( $A_m$  is the true projected contact area measured at  $h_m$ ) can be considered as the hardness ( $H$ ) of the indented material. Upon unloading, the  $P$ – $h$  slope is initially linear,  $\left.\frac{dP_u}{dh}\right|_{h_m}$ , where  $P_u$  is the unloading force. Upon complete unloading (zero load), the residual depth is  $h_r$ . The areas underneath the loading curve and unloading curves are the total work done by loading  $W_t$  and released by elastic unloading  $W_e$ , respectively. Thus, the area enclosed by the loading and unloading curve is the (plastic) work done by the indentation process,  $W_p = W_t - W_e$ . These experimentally accessible parameters are used to extract elastic and plastic properties of the indented material, and provide the basis for the algorithms included in most commercial indenters for property extraction. With this background, we now briefly describe specific approaches to measure properties using sharp indentation (see Fig. 3).

## 2.2. Evaluating elastic modulus using instrumented indentation

The method proposed by Oliver and Pharr [37] is by far the most common approach to determine modulus (and hardness) via interpretation of  $P$ – $h$  behavior. Some related earlier efforts can be found in Refs. [16,38]. There have been a number of comprehensive reviews recently on this topic [10,12,13].

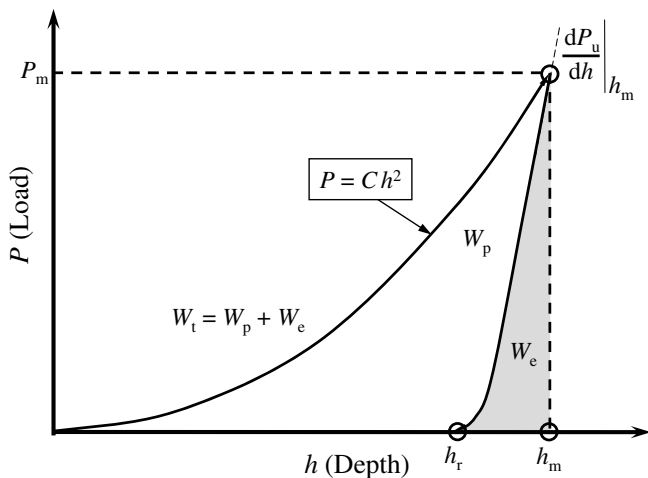


Fig. 2. Schematic of load–depth ( $P$ – $h$ ) curve during sharp indentation of a ductile material. See text for details.

The original method is based on the expression

$$E^* = \frac{1}{\beta} \left. \frac{dP}{dh} \right|_{h_m} \frac{1}{2} \frac{\sqrt{\pi}}{\sqrt{A_m}}, \quad (2a)$$

where  $\beta$  is a correction factor and  $E^*$  is the reduced modulus defined as

$$E^* = \left[ \frac{1 - \nu^2}{E} + \frac{1 - \nu_i^2}{E_i} \right]^{-1}, \quad (2b)$$

where  $E_i$ ,  $\nu_i$  are the Young’s modulus and the Poisson ratio of the indenter, respectively. The projected contact area is given as

$$A_m = \pi a_m^2 = \pi h_c^2 \tan^2 \theta, \quad (3)$$

where  $h_c$  is defined as the contact depth and is given by the relation

$$h_c = h_m - \gamma P_m \left/ \left. \frac{dP_u}{dh} \right|_{h_m} \right. \quad (4)$$

and  $\gamma$  is a tip-dependent geometry factor (typically denoted as  $\epsilon$  but we change the variable here so as not to confuse this with strain), which is equal to 0.72 for a conical, 0.75 for a parabola of revolution and 1 for a flat cylindrical punch indenter. Here  $\left.\frac{dP_u}{dh}\right|_{h_m}$  can be evaluated via a power law fitting function of the unloading curve [13,37] or the continuous stiffness measurement (CSM), in which a number of partial unloading steps are superimposed on the loading curve [13].

For the method to work satisfactorily, careful calibration of the machine compliance, identification of the first indenter–surface contact point, and determination of the area function are all very important factors [10,12,13].

There are, however, two outstanding issues remaining for further investigations. The first is that this method does not rigorously account for pile-up (or sink-in) [13], and an experimentally proven correction scheme is needed. Another important issue is the value of the correction factor  $\beta$  used in Eq. (2). For a Berkovich indenter, the commonly used values in the available literature are between 1.034 and 1.09 [10,13]. An accepted consensus on  $\beta$  requires thorough three-dimensional (3-D) computational investigations. Nevertheless, this method is a mainstay of indentation-based research, and the “indentation modulus” is a descriptor not only of material stiffness, but of microstructural features as well (see Section 7).

## 2.3. Evaluating plastic stress–strain behavior using instrumented indentation

Mathematical expressions to predict indentation  $P$ – $h$  curves using known elastic–plastic properties as input were explicitly developed for Vickers [39] and Berkovich [40] indenter tips using 3-D finite element analysis (FEA), i.e. the “forward problem”. Following this, an explicit step-by-step methodology [16] was outlined for estimation of elastic–plastic properties from instrumented sharp indentation (the “reverse problem”) with detailed guidelines and

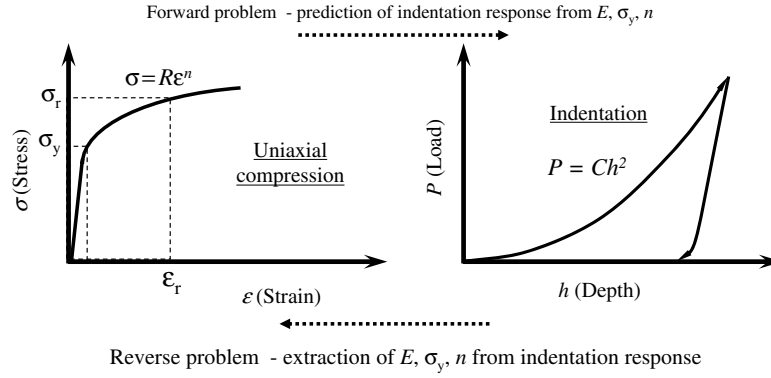


Fig. 3. Graphic depiction of forward and reverse indentation analyses.

sensitivity analysis in Ref. [41]. On a related note, using large deformation FEA and dimensional analysis [42] on the sharp indentation problem, Cheng and Cheng (see Ref. [9] for a review) have obtained a significant amount of useful information linking material properties to indentation characteristics (such as loading curvature, initial unloading slope, work ratio and depth ratio). Finally, proposing a new way to define representative stress and strain, Dao et al. [8] first constructed a complete set of explicit analytical functions based on large deformation FEA to extract both elastic and plastic properties from indentation curves, and then proposed a reverse analysis algorithm. We briefly outline the approach here.

For computational simplicity, models were performed using an axisymmetric analysis; a pyramidal (Berkovich) tip was represented by a shallow cone with identical projected area. The chosen materials were isotropic, Hookean elastic and power-law plastic, as shown in Eq. (5)

$$\sigma = \begin{cases} E\varepsilon, & \text{for } \sigma \leq \sigma_y, \\ R\varepsilon^n, & \text{for } \sigma \geq \sigma_y, \end{cases} \quad (5)$$

where  $R$  is a strength coefficient,  $n$  is the strain hardening exponent and  $\sigma_y$  is the initial yield stress at zero offset strain. Using the continuity at the initial yielding and the assumption that total strain  $\varepsilon$  is composed of yield strain  $\varepsilon_y$  and plastic strain  $\varepsilon_p$ , or  $\varepsilon = \varepsilon_y + \varepsilon_p$ , Eq. (5) can be rewritten for  $\sigma > \sigma_y$  as

$$\sigma = \sigma_y \left( 1 + \frac{E}{\sigma_y} \varepsilon_p \right)^n. \quad (6)$$

The derived expression is used to define a representative stress  $\sigma_r$  at  $\varepsilon_p = \varepsilon_r$ .

The importance of the representative value can be explained simply as follows. Under sharp indentation, the material immediately experiences large strains. Thus, it is unlikely that deformed regions near the indenter tip (and thus contributing most strongly to loading curvature  $C$ ) are precisely at their yield point. It can be argued that  $n$  is more readily accessible from the relationship of  $W_p$ ,  $W_t$  (or of  $h_r$ ,  $h_m$ ) as the extent of elastic springback will depend on hardening. Assuming  $E$  can be extracted via

the methods in Section 2.2, it only remains to extract a representative stress  $\sigma_r$  from  $C$ . This is at the heart of the work described herein.

A parametric study spanning a range of useful engineering solids (76 combinations of  $E$ ,  $\sigma_y$  and  $n$  detailed in Appendix A of Ref. [8]) was analyzed with dimensional analysis in order to establish closed-form analytical functions that related the input parameter spaces of elastic–plastic properties ( $E$ ,  $\sigma_y$  and  $n$  in Eq. (5)) to the output parameter spaces of  $P$ – $h$  characteristics ( $C$ ,  $\frac{dP}{dh}|_{h_m}$  and  $\frac{h_r}{h_m}$  defined in Fig. 2). Once those functions were identified, the forward and reverse algorithms of indentation were constructed upon the most robust and least sensitive route. Of all the dimensionless functions found, the most critical one was derived from the concept of representative stress for the description of loading curvature as follows:

$$\Pi_1 \left( \frac{E^*}{\sigma_r}, n \right) = \frac{C}{\sigma_r}. \quad (7)$$

It was shown that  $\Pi_1$  increases with increasing  $n$  for representative strain  $\varepsilon_r < 0.033$  and decreases with increasing  $n$  for  $\varepsilon_r > 0.033$ . However, when  $\varepsilon_r = 0.033$  an explicit functional form of  $\Pi_1$ , independent of hardening exponent  $n$ , was given [8]

$$\begin{aligned} \Pi_1 \left( \frac{E^*}{\sigma_{0.033}} \right) &= \frac{C}{\sigma_{0.033}} \\ &= -1.131 \left[ \ln \left( \frac{E^*}{\sigma_{0.033}} \right) \right]^3 \\ &\quad + 13.635 \left[ \ln \left( \frac{E^*}{\sigma_{0.033}} \right) \right]^2 \\ &\quad - 30.594 \left[ \ln \left( \frac{E^*}{\sigma_{0.033}} \right) \right] + 29.267 \end{aligned} \quad (8)$$

which fits all 76 data points within a 2.85% relative error. Hence, a representative strain of  $\varepsilon_r = 0.033$  (3.3%) was identified, and defined as the plastic strain level that yields the loading curvature independent of material's hardening behavior (other values of representative stress and strain obtained in the literature were also discussed and related to  $\varepsilon_r = 0.033$  [16,39,43–46]). The significance

of this representative stress (or strain) concept is twofold. For the forward analysis, regardless of how two materials strain-harden, as long as those materials possess the same stress at 3.3% plastic strain, the indentation loading behavior will be identical. On the other hand, for the reverse analysis, Eq. (8) implies that by knowing only  $E^*$  and experimentally measuring  $C$  from the indentation response, one plastic parameter ( $\sigma_{0.033}$ ) of the indented solid can be robustly estimated without the knowledge of material's hardening behavior. As mentioned above, a similar dimensionless function  $\Pi_2$  was provided to extract  $n$  from  $\left.\frac{dP_u}{dh}\right|_{h_m}$ , after calculation of  $E^*$  and  $\sigma_{0.033}$ . Using Eq. (6),  $\sigma_y$  and thus the full elastic–plastic behavior of the material, may be obtained [8].

In brief, the forward algorithm was robust with low sensitivity while the reverse algorithm was robust in predicting the representative stress  $\sigma_{0.033}$  but suffered high sensitivity in predicting  $\sigma_y$  and  $n$ . Also uniqueness of the solution is not always guaranteed at certain parameter ranges [8,9]. In order to circumvent the high sensitivity in extracting properties from indentation, various models of neural network (e.g. inverse analysis) have been used for both conical [47,48] and spherical [19,49] indenters for more complex systems such as film/substrate and graded materials.

Another well-received solution to enhance the capability of reverse analysis was the use of two or more indenters [14,15,50–53]. In fact, the idea of using multiple tip geometries to mechanically characterize elastic–plastic solids dates back to works by Dugdale [54,55] and Atkins and Tabor [56]. In addition, various ways to construct universal dimensionless functions have been explored by combining dimensional analysis and FEA computations. For example, among many others, Cao et al. [44] proposed an energy-based formulation, and Wang et al. [50,57], using the non-dimensional parameter  $A = P/hS$  (where  $S = \frac{dP_u}{dh}$  is contact stiffness) that can be monitored via continuous stiffness measurement (CSM) during indentation test, constructed a reverse algorithm relating elastic and plastic properties to  $\sigma_y$  and  $n$ .

#### 2.4. Summary remarks

As described above, a remarkable effort has been expended to extract the properties of engineering metals using indentation methods. This has spurred a number of related activities to determine the limits of applicability of these analyses, in the context of size scale and material type (see below). In addition, methods have provided a springboard for the investigation of heterogeneous materials systems. We describe progress on this latter topic in the next section.

### 3. Indentation response of heterogeneous material systems

As stated in Section 1, one advantage of indentation is the ability to probe the mechanical response of systems that are inaccessible via other methods. Most notably, this includes thin or thick films on substrates, multilayers or particulate composites. Nevertheless, although these finite systems may be readily indented (Fig. 4(a) shows an example of indentation of a patterned metallic line on a substrate [58]), interpretation of results has required significant analysis. The study of contact response in finite layers (e.g. indentation of an elastic strip on a rigid surface) can be found in the civil engineering literature, back to the turn of the century (see Ref. [1] for a review.) A far more recent concern has been the differentiation of coating and substrate contributions to indentation response in bilayer systems. That is to say, during nanoindentation of a thin film on a substrate (Fig. 4), if indentation depth is of the order of film thickness, the elastic and plastic properties of both constituents as well as interface quality affect the loading and unloading behavior. However, as many commercial indenter systems include automatic algorithms to calculate hardness and modulus, most studies in the literature have focused on these resultant values, and not the raw  $P$ – $h$  response. Comprehensive treatment of the subject may be found in Refs. [59,60]. In this section, we discuss two further heterogeneous systems: multilayered materials [61–71] (3.1) and hard particle/soft matrix composites

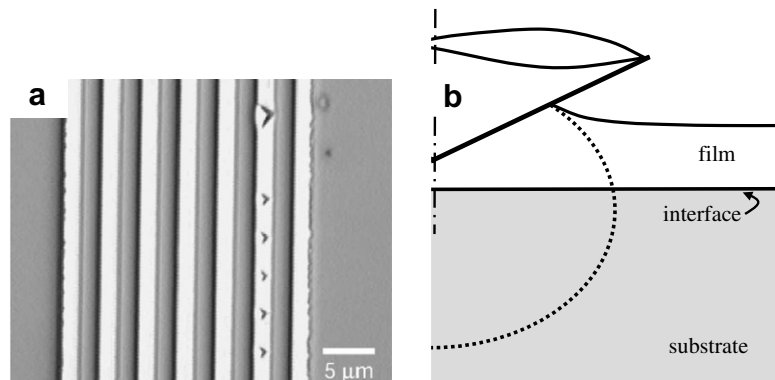


Fig. 4. (a) Nanoindentation of patterned metallic lines on a substrate, illustrating the flexibility of the technique [58]. (b) During indentation of a film on a substrate, the composite response of both constituents must be considered for large depths.

(3.2), namely the effect of different constituents on combined indentation response. Section 3.3 is devoted to the probing of local properties.

### 3.1. Indentation analysis of multilayered materials

To begin, we consider a structure composed of alternating layers of two perfectly bonded metals, designated A and B, of equal thickness and with elastic–perfectly plastic responses (used as input in the model), and  $\sigma_{yB} > \sigma_{yA}$ . This composite is indented normal to the layer direction with a sharp indenter, as shown schematically in Fig. 5. The indentation displacements considered are sufficiently deep that the effective hardness resulting from the composite structure can be obtained. Note that although in reality the individual layer thickness may be conceived to be in the submicron range, there is no intrinsic length scale involved in this continuum-based simulation. As a consequence, there is no size-dependent effect caused by the varying underlying deformation mechanisms found in actual micro- and nanolayered metals. Nevertheless, it can be argued that a continuum understanding is the first step, and once a robust description at this level is obtained, any deviations arising from micro- or nanostructural effects may be readily analyzed. Specifically, we consider the indentation response of such a structure, and discuss the effectiveness of homogenized composite properties in describing the results.

Finite element analyses of compressive loading are first performed to obtain the overall effective yield strength of the A–B multilayered composite. The effective stress–strain response in the transverse direction is then used as the input response of a homogeneous material to be subjected

to indentation loading, the results of which are compared to indentation models of multilayers themselves. Two models are considered (Fig. 5, insets), with the topmost layer either material A or B, named “AB stack” or “BA stack”, respectively. (In the case of indenting a homogeneous material having the built-in composite properties, as described in the previous paragraph, the entire specimen is simply replaced by a homogeneous material with the specified elastic–plastic input response.) Other modeling details can be found in Ref. [72].

Fig. 5 shows the modeled hardness as a function of indentation depth for the homogeneous A and B materials, the homogenized multilayer, and the composite structures with explicit A–B layering. It is seen that the model of homogenized multilayers results in hardness values which are almost exactly the averages of pure A and B materials. One can calculate the ratio of hardness/yield strength for the homogeneous materials and homogenized multilayers, and the ratio is approximately 2.93 for all three models.

As for the composite structures in Fig. 5, it is evident that the “AB stack” and “BA stack” models do not generate the same hardness results as in the homogenized multilayers. At shallow depths, the hardness is dominated by the top layer material so “BA stack” and “AB stack” result in very high and low hardness values, respectively. As the indentation depth increases, the difference between the two arrangements is reduced and the two curves tend to merge. Ideally there will be a single hardness value at very large indentation depths, although in Fig. 5 the two curves are still somewhat apart at a depth corresponding to eight initial layer thicknesses. Nevertheless, it is apparent that both composite models underestimate the overall strength of the structure (recall that the homogenized model represents the “true” composite response, or, in other words, it is the continuum representation of the multilayers under uniaxial loading). If the measured hardness is to be used to derive the overall yield strength of the multilayers, a ratio smaller than that identified for homogeneous materials (2.93 as shown above) should be used.

One factor that can contribute to the underestimation of composite yield strength by indentation is the localized nature of indentation loading; the several softer layers close to the indent accommodate a greater part of the geometric constraint through easy plastic flow. This also implies a less efficient load transfer process during indentation compared with the case of overall uniaxial loading of the composite. It should be noted that the present example concentrates only on alternating layers of elastic–perfectly plastic metallic films. If one or both materials strain-harden upon yielding, the indentation response can be significantly influenced depending on the actual hardening parameters. Nevertheless, this example serves to provide a baseline understanding of the relationship between indentation hardness and overall yield strength for multilayered elastic–plastic materials. It also serves to illustrate the rather poor current status of knowledge on the indentation behavior of even this very simple form of heterogeneous material system. Further

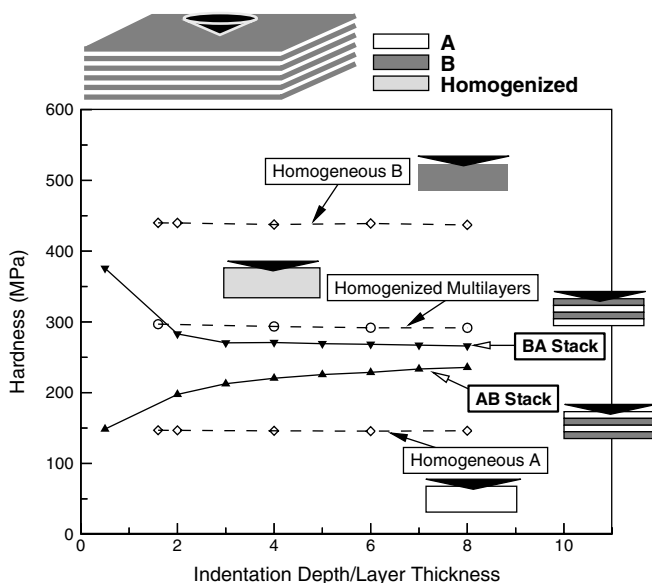


Fig. 5. Top schematic shows indentation of an A–B multilayered composite. Plot shows indentation hardness as a function of normalized depth for A–B and B–A stacks (see inset), as compared to homogeneous A, B, and homogenized composite [72].

explorations involving more complex material, geometric and interface features need to be undertaken.

### 3.2. Hard particles/soft matrix systems

A similar methodology has been applied to a composite containing hard particles in a ductile matrix [73,74]. Material systems of this type include particle-reinforced metal matrix and polymer matrix composites, dispersion-strengthened alloys and precipitation-hardened alloys. Here global loading (uniaxial tension or compression) of a model composite with discrete hard particles inside a soft, elastic–power law plastic hardening matrix can be modeled using finite elements. The resulting stress–strain behavior can then be used as the input of a homogeneous material, to be subjected to indentation modeling, and compared with direct indentation of the two-phase composite [75].

Numerical results have shown that, similar to the multi-layered case, the indentation behaviors of these two models differ significantly [73,74]. The two-phase composite (with particles explicitly accounted for) consistently shows a harder response than the corresponding homogenized composite, even when the indent size is much greater than the size and spacing of the particles. From the simulation it can be observed that there is an increased particle concentration (“particle crowding”) directly underneath the indentation in the particle-containing model, which cannot be easily accounted for in the homogenized model. Fig. 6 shows a representative deformed two-phase composite under indentation and the plastic strain contours. The “particle crowding” effect may be partially explained by

the very high hydrostatic pressure below the indentation. The presence of hydrostatic pressure implies greater volumetric compression for the soft matrix than for the much stiffer particles. This, in turn, means a relatively higher particle volume fraction. As the indenter moves downward, it encounters resistance from a material with an increasingly greater concentration of hard particles. This increase in particle concentration also renders the locally work-hardened matrix even more constrained. A greater load is thus needed to achieve a given indentation displacement. In the homogenized model, this hardening effect due to particle crowding is non-existent. The main implication is that, in actual indentation tests, the indentation hardness can overestimate the overall strength of the composite. Experimental measurements using macro-indentation on SiC particle-reinforced Al matrix composites have provided support of the above modeling results [75]. Although the experiments were performed on materials with micro-scale heterogeneity using large indentation, similar behavior is expected when performing nanoindentation on materials with nanoscale heterogeneity or even well-characterized precipitation-hardened engineering alloys.

It is worth pointing out that a similar kind of particle concentration enhancement has also been experimentally observed in post-indented specimens [76]. Detailed quantitative metallography was performed on an Al/SiC composite, which showed a distinct increase in particle concentration directly beneath the indentation even after the disengagement of the indenter. This is due to the residual compressive stress field remaining in the material after unloading, also illustrated by the finite element analysis. Finally, it has also been shown numerically that indentation of a material containing internal pores behaves in precisely the opposite manner to the above two-phase composites. That is to say, under indentation, local pore crushing occurs, leading to underestimation of the overall mechanical strength [77].

### 3.3. Local indentation behavior in heterogeneous materials

The examples given in Sections 3.1 and 3.2 belong to the cases where the indentation size is greater than the microstructural feature size in the heterogeneous materials. In practical applications, nanoindentation is frequently employed to probe a particular micro- or nanoscale entity in a multiphase structure. The indentation response may thus be influenced by the microscopic heterogeneity, even though the indentation is strictly within one nominally homogeneous feature. Durst et al. [78] have used finite element simulations to investigate the influence of the shape and aspect ratio of particles on the single-phase indentation behavior in particle–matrix systems. The simulation results rationalized the transition indentation behavior from particle to matrix, experimentally observed in precipitation-hardened nickel-based superalloys. Olivas et al. [79] have recently used nanoindentation to study the thermal residual stresses in SiC particle-reinforced Al matrix composites. The technique, originally developed by Swadener

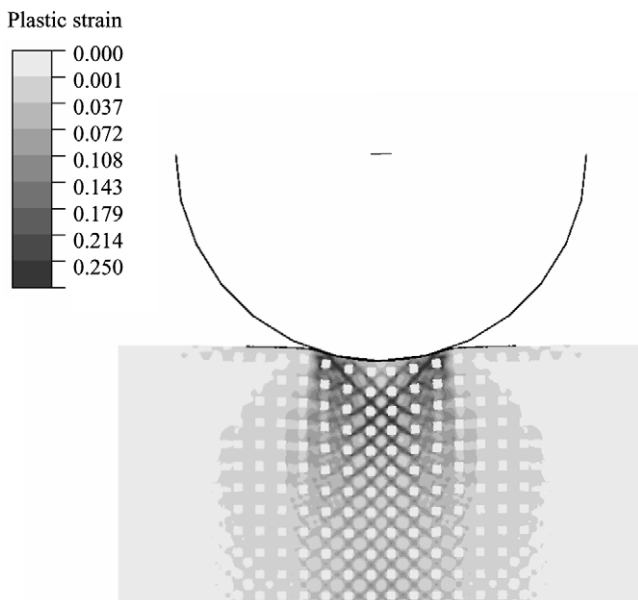


Fig. 6. Contours of equivalent plastic strain in a representative 2-D “two-phase composite” model under indentation [75]. The particles were taken to be elastic with no plastic strain so they are discernible in most of the regions. Plastic flow inside the matrix is forced into a banded structure. The interparticle spacing directly underneath the indenter is reduced, compared to the lightly loaded regions.

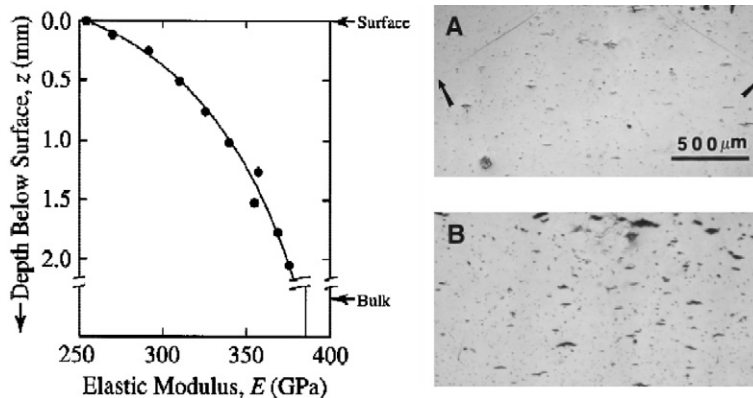


Fig. 7. Left plot shows power-law grading elastic modulus of a material, with decreasing compliance away from the surface. Right figure shows (A) characteristic cone cracking in a homogeneous composite under spherical indentation (from top, not shown) and (B) suppression of cracks in a FGM with graded modulus [81].

et al. [80], features extrapolation of spherical indentation data from the post-yield regime to determine the contact radius at the onset of yielding. The experimental results compared favorably with the finite element analysis, which suggested the general credibility of applying spherical nanoindentation in characterizing the local surface residual stress in the ductile matrix in metal matrix composites. Clearly, the effect of microstructural heterogeneity on the local indentation response is still an under-researched area. More work should be conducted to increase the applicability of nanoindentation in accurately probing the mechanical behavior in realistic material systems.

### 3.4. Functionally graded materials and limiting assumptions

Functionally graded materials (FGMs) are a relatively new class of structure theoretically purported to reduce the process and/or operation-induced stress concentrations typically present in composites with discretely heterogeneous structures. As many proposed FGMs exist in coating form, similar limitations arise in probing their mechanical behavior, and indentation emerges as a preferred method. As stated above, extraction of the depth-dependent elastic–plastic properties of graded metallic systems using indentation has primarily been studied using neural network methods and inverse analysis [16–22,46–48]. In addition to property extraction, interesting results have been obtained regarding the contact (tribological) response of FGMs (e.g. Refs. [81,82]). For example, fabrication of a graded alumina–glass composite in which Young’s modulus increased with depth showed a complete suppression of Hertzian cone cracks underneath spherical indentation [82] (Fig. 7). This innovation provided new possibilities for improving contact-damage resistance in engineering ceramic materials [83–87]. However, these results were difficult to exploit using conventional deposition techniques, e.g. thermal spray [88], primarily due to the imperfect load transfer between composite phases. This is an important consideration for the expansion of indentation analysis

for real graded systems, as well as heterogeneous structures.

### 4. Departures from continuum treatment – the indentation size effect

The above discussions focus on the continuum treatment of indentation experiments and do not include any intrinsic material length scales. However, it is now well established that bulk microcrystalline or single-crystal materials exhibit an “indentation size effect” (ISE) in which hardness increases with decreasing sampling volume. For the purposes of this short commentary, considering a Berkovich indenter, we may distinguish between two nanoindentation responses exhibiting ISE.

The first, with maximum depths ranging between 400 and 10000 nm, results in a continuous  $P$ – $h$  curve, with steadily decreasing hardness at larger depths. In the absence of a depth-sensing system, this effect is exhibited under microhardness tests, with decreasing  $P/A$  under increasing load, measured optically (e.g. Refs. [89–94]). A number of researchers have attempted to address this effect via the phenomenological explanation that in these experiments the dominant length scales of indentation deformation approach critical microstructural length scales of dislocation spacing. Although qualitatively a general agreement has been reached on this topic, quantitative agreement has not yet been achieved, despite a large amount of modeling activity [95–98]. Interestingly, the ISE is not exhibited to nearly as great an extent in nanocrystalline metals [99,100], ostensibly due to the far smaller critical length scale (grain size) involved in plastic deformation. Further comment on this particular topic (nanocrystalline metals) is provided in the accompanying review in this issue [101].

The second ISE response occurs at maximum depths of less than 400 nm, and does not so much concern the change in hardness with indentation depth, but rather the discretization of deformation into its elastic and plastic components. This is manifested by a “staircase”-shaped

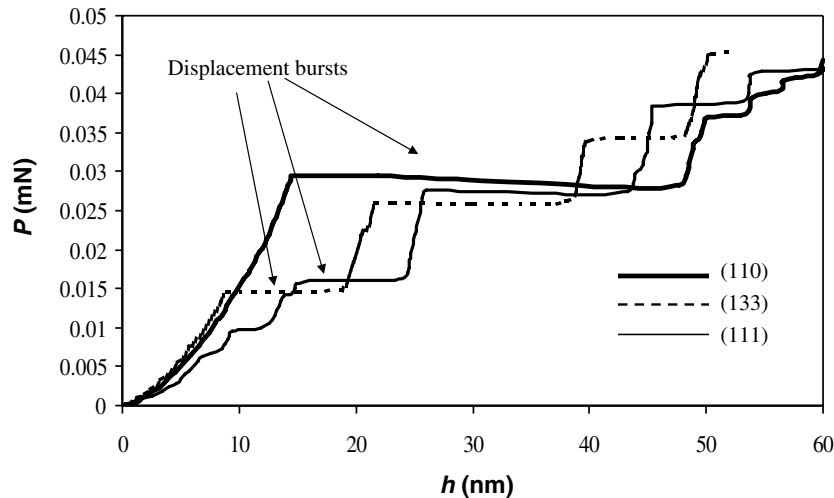


Fig. 8.  $P$ - $h$  data from nanoindentation of single-crystal Al thin films ( $t = 400$  nm) of different orientation on Si substrates [102]. Curves show the characteristic “staircase” structure resulting from discretization of elastic (regions of positive slope) and plastic (horizontal lines: displacement “bursts”) deformation under load control. Much of the work in the following sections of this paper has been undertaken to understand this phenomenon.

$P$ - $h$  curve, as shown in Fig. 8. Two salient features of this curve are the following: (i) the initial positive slope corresponds to the response of a purely elastic material (with the modulus of the indented specimen) under spherical indentation (with tip radius  $R$  equal to that of the Berkovich indenter – see Fig. 1(c)), and (ii) the first displacement burst (or “pop-in”) typically occurs at a load  $P$  that corresponds to the maximum shear stress under the indenter of the same order as the theoretical shear strength of the indented specimen material. Thus, the underlying mechanism for this is the nucleation and propagation of dislocations, under an initially elastic strain field. This phenomenon has been observed in bulk and thin film single and polycrystals (e.g. Refs. [102–120]) and a review of experimental techniques can be found in Ref. [121]. It should be noted that although initial efforts to describe this behavior focused on perfectly smooth surfaces, a number of recent investigations have pointed out the importance of asperities as sites for dislocation initiation (see Section 5). To further explore the effect of specimen size on behavior, nanoindentation (or nanocompression employing position control of nanoindenters) has been performed on structures with small volume dimension in all three directions, e.g. Si nanospheres [122,123], Au nanoclusters [124] or pillars [125–127] and Ni-based microspheres [128]. These latter studies are notable in that the researchers were able to delineate size-effect observations without the high strain gradients inherent to indentation.

Since its initial observation, a tremendous effort has been made to understand the nature of defect nucleation under nanoindentation. Beyond the issue of tribology and/or engineering systems at the nanoscale, the rationale for this extends to a clarification of the fundamental nature of plasticity itself. Although a number of conceptual models have been proposed to describe this, it has been accepted that for a true picture, we must turn to atomic-

scale models and direct in situ observation of defect formation under nanoindentation – the foci of the next two subsections, respectively.

## 5. Atomistic modeling of nanoindentation

### 5.1. Comprehensive review of the literature

Atomistic modeling means utilizing discrete atomic coordinates as (one of) the essential degrees of freedom in modeling material behavior [129]. While molecular dynamics (MD) simulation is a well-known atomistic method, it is important to recognize there are many other discrete-atom based techniques such as static energy minimization, chain-of-states approach [130–133] for saddle point calculation [134,135], Monte Carlo, hyper-MD [136], etc., that ameliorate some of the serious deficiencies of MD. The potential energy surface (PES) that drives atomistic dynamics in the computer may be an empirically fitted function [137], or it could be evaluated on-the-fly by solving concurrently the quantum mechanical problem of the electrons [138]. Most atomistic models of nanoindentation to date have been carried out with empirical potentials [58,139–177], but there are also some notable exceptions [178–182]. The goals of these simulations are similar: to reveal the inelastic deformation mechanisms under the indenter, to visualize the defect structures and to interpret the  $P$ - $h$  curves.

To our knowledge, Landman et al. [139] and Hoover et al. [140] performed the first atomic-level simulations of nanoindentation. The latter in particular were interested in using these simulations to probe bulk elastic–plastic responses [140,143,183]. Harrison et al. published simulation results of nanoindentation on diamond (111) surface [141,184], and found a fracture mode of stress relaxation under the indenter. Harrison, Brenner, Sinnott et al. then

published a series of papers on indentation, adhesion and friction in covalent materials, using more realistic interatomic potentials [145,185,186].

In 1998, Kelchner, Plimpton and Hamilton published a landmark paper on the dislocation structure generated under the Au(111) surface after indentation by a smooth sphere [146]. Unlike previous studies, they paid close attention to characterizing the bulk atomic environment for defect visualization. They invented a scalar measure – the centrosymmetry parameter – for each atom, to distinguish between partial and perfect dislocation configurations inside a face-centered cubic (fcc) crystal. Their calculations showed for the first time that the initial dislocations nucleated in spherical indentation do not originate from the surface, but directly inside the bulk, away from any pre-existing defects – in other words, homogeneous nucleation. This was later verified by Gouldstone et al. in a bubble-raft experimental model (Fig. 11) [188]. A soft-phonon criterion [129] was proposed to address the stress condition required for homogeneous nucleation in the athermal ( $T = 0$  K) limit (Fig. 9). Specifically, an analytical criterion was derived to describe soft long-wavelength phonon or elastic wave initiated instability [154,161], although this did not exclude other phonon modes [189]. An immediate consequence of this explanation is that the raw magnitude of the experimentally measured strength before the first displacement burst in nanoindentation appears to be a very significant fraction of the theoretical strength [190–192], the upper bound on material strength. A large body of work appeared thereafter, mostly probing the athermal limit (with and without pre-existing defects).

Much attention has been focused on the responses of grain boundaries (GBs) under an indenter [193]. Feichtinger et al. observed GB sliding, and GB acting as a dislocation sink in their simulation [155]. Ma and Yang observed GB-aided partial dislocation nucleation – in other words heterogeneous nucleation [161] – which has a lower athermal threshold stress than that of homogeneous nucleation inside the perfect lattice [159]. Yoon, Kim and Jang observed lattice dislocation absorption induced GB migration [194]. The generally complex interactions of lattice dislocations with GB and GB dislocation networks have been seen by Hasnaoui et al. [164], in qualitative agreement with uniaxial tension simulations. The nanoindenter in these simulations can be regarded as a “dislocation gun”, via which plasticity is injected into a localized region. One can interrogate local responses, such as near GB vs. inside the grain interior [159,193], rather than measuring the average effect, as in uniaxial tension simulations.

While nanoindentation experiments are often analyzed in the context of bulk properties, surface phenomena and surface effects are important, and atomistic simulation is a powerful tool for revealing these, since the physical effects of surface stress, lattice anisotropy and the possible complexities of the geometry itself are automatically built in. Zimmerman et al. studied the significant effect of a single atomic step (asperity) on the surface in lowering the ather-

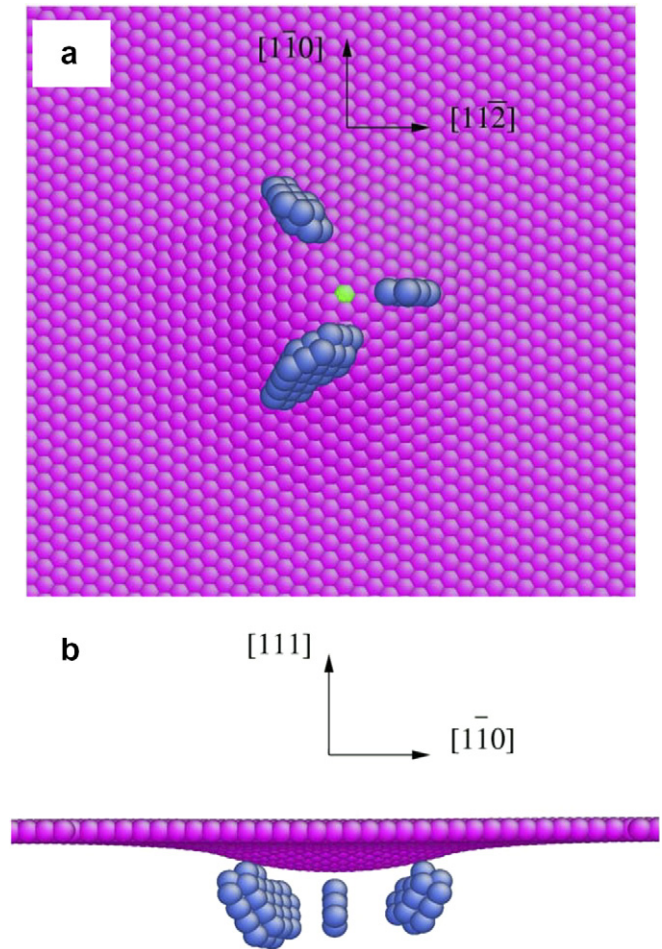


Fig. 9. MD simulation of nanoindentation of fcc Cu by a spherical indenter. Atomic structure of homogeneously nucleated dislocations beneath the (111) surface: (a) bottom view along the  $[111]$  direction; (b) side view along the  $[112]$  direction. Atoms with a coordination number other than 12 are shown. The indenter first contacts the green atom. The sites of subsurface homogeneous dislocation nucleation agree well with nonlinear elasticity finite-element calculation using the Cauchy–Born rule and soft-phonon criteria. (Reprinted with permission from Ref. [204].) (For interpretation of the references in colour in this figure legend, the reader is referred to the web version of this article.)

mal threshold load of heterogeneous dislocation nucleation [152]. Smith et al. used atomistic simulation to study material pileup patterns when indenting the (110), (100) and (111) surfaces of body-centered cubic (bcc) Fe, and found good qualitative agreement with experiments [160]. The same pileup pattern problem was also studied by Wang et al., but with continuum crystal plasticity [195].

For ceramic materials, detailed modeling have been carried out to predict, for example, phase transformation [169,180,196], cleavage fracture and solid-state amorphization [150,162] under indentation. Studies by Szlufarska et al. showed, for nanocrystalline ceramics, the importance of the thin GB amorphous layer in grain sliding and rotation [175,176]. Simulation of nanoindentation on a model bulk metallic glass was recently performed by Shi and Falk, who observed intense shear localization leading to multiple

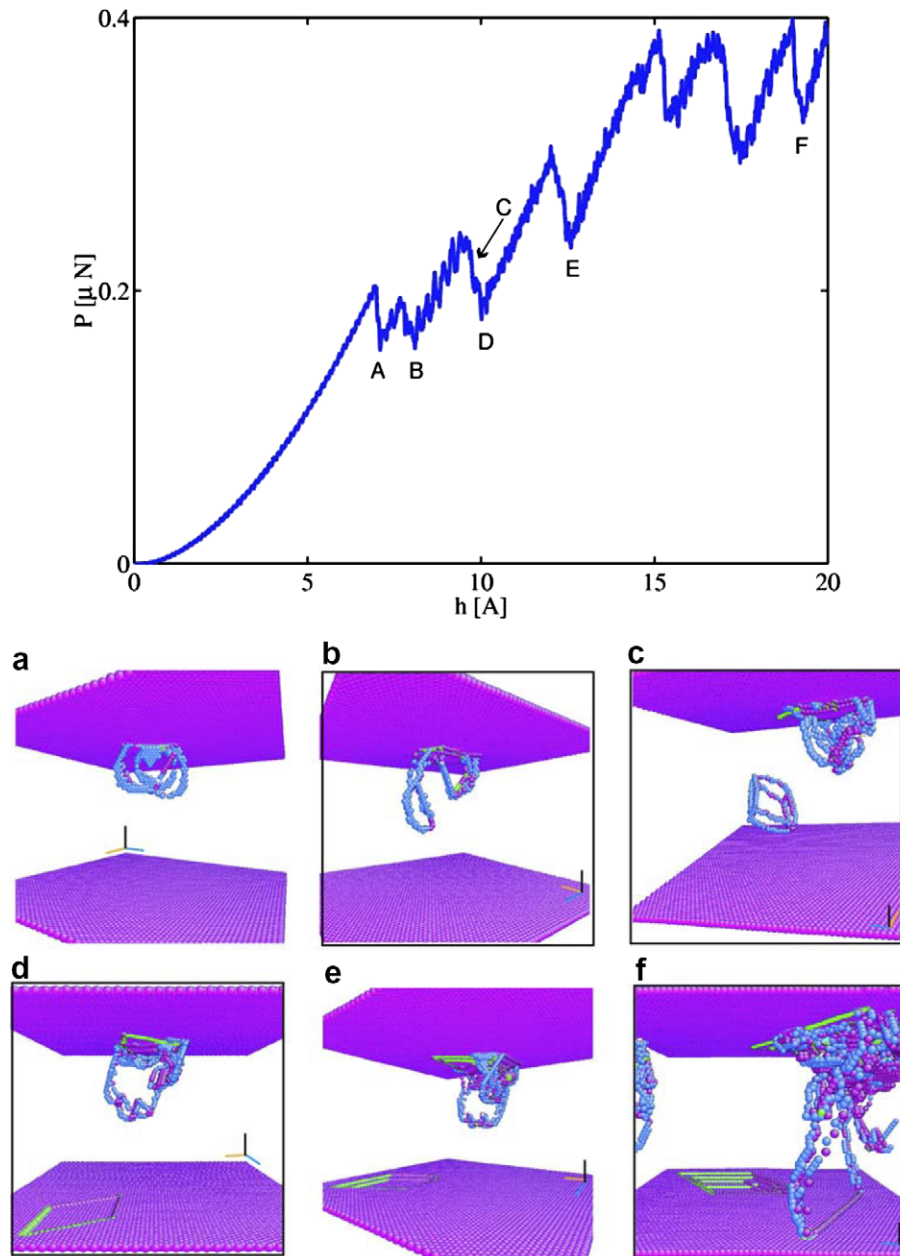


Fig. 10. Correlation of the MD  $P$ - $h$  response and dislocation activities in single-crystal fcc Al at several indenter displacements. Atoms with a coordination number other than 12 are shown. Note the heterogeneous nucleation of a full prismatic dislocation loop at (c). (Reprinted with permission from Ref. [161].)

shear band nucleation [172]. Nanoindentation simulations of a polymeric material [197] and a protein crystal [198] have been performed by coarse-grained molecular dynamics where the discrete degrees of freedom represent groups of atoms (structural units) rather than individual atoms, which interact with each other via effective coarse-grained potentials. Very recently, an experimental colloidal crystal indentation model was constructed by Schall et al. [187], and visualized by laser diffraction microscopy and confocal microscopy, following prior work by Gouldstone et al. [188] and Thalladi et al. [199]. The novel feature of this “atomic-scale” model is that the role of thermal fluctua-

tions in homogeneous and heterogeneous defect nucleations can now be systematically studied. A stacked straw model was also recently used for experimental simulation of crystal defect mechanisms under indentation [200].

### 5.2. Commentary on future opportunities for research

Generally speaking, atomistic modeling faces three challenges in trying to fulfill its stated goals: (i) the accuracy of the PES description, (ii) the length scale and (iii) the time-scale that can be modeled. As we will see, none of these challenges are insurmountable, if one does not insist on

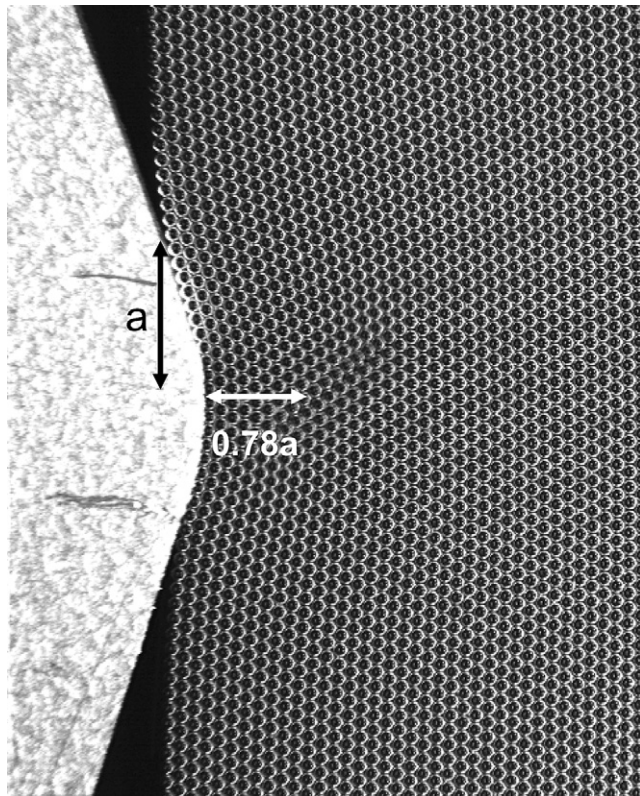


Fig. 11. Photograph of a bubble-raft model that provides a 2-D experimental analog of atomic models. In this figure, indentation with a blunt tip causes homogeneous nucleation of a dislocation at the location of maximum shear stress predicted by Hertzian theory for elastic solids [188].

using a single atomistic approach (such as MD), and is willing to link to models at other scales such as discrete dislocation dynamics [173,201,202] and continuum dynamics [181,182]. However, practically speaking, among the three challenges, that of the timescale is currently the most daunting. For the PES description, fairly robust empirical potentials now exist for monatomic metals, such as Cu [203,204], that allow one to carry out basic mechanistic studies to compare with experiments. While at present there is definitely a length scale challenge, one could argue that nanoindentation is probably one of the best problems in mechanics for atomistic models, since the actual indenter tip radius is of the order of 1–1000 nm. Nowadays one can easily perform atomistic calculations for a  $10^6$  atom configuration, which corresponds to a  $23 \times 23 \times 23$  nm cube of copper, on a personal computer. An optimistic extrapolation of Moore's law in computing power, combined with smart treatments of the surrounding continuum [205] and mesoscale [206], suggest that the length scale challenge for atomistic simulation is not as a daunting problem as it initially seems. Furthermore, an argument can be made that atomistic models probably should not be used above 100 nm in an engineering setting, since that is the domain of mesoscale dislocation dynamics [201,202,207] and continuum crystal plasticity and damage mechanics [195,208],

which are far more aesthetically appealing descriptions at those scales.

However, there is a real timescale challenge for atomistic models [137], since the actual nanoindentation measurements take seconds to complete, while the most common atomistic approach, MD simulation, tracks events on the picosecond timescale (i.e. atomic vibrations). In addition, present in situ observations (see Section 6) do not acquire images fast enough to resolve many of the transient dislocation activities, so atomistic simulations can fill in those details. However, one must keep in mind that what one “sees” in an atomistic simulation does not necessarily reflect experimental reality. Additional analytic theory is necessary to justify results.

For example, in the case of indenting a pristine single crystal with atomically flat surface [188], the first inelastic displacement burst at low temperature may correspond to homogeneous defect nucleation in the bulk, defined as nucleation without the aid of pre-existing lattice defects. The athermal threshold condition of homogeneous nucleation has been proposed to correspond to locally soft phonons [189,192,209], where the vibrational frequencies of some normal modes of the perfect crystal take on imaginary parts due to the high stress. A special case of the general soft phonon instability [189,192,209] is the long-wavelength soft phonon instability [154,161,189,210], which admits an elegant analytical criterion that corresponds to vanishing of the local acoustic tensor [185,211,212]. This athermal limit of soft phonons (whether it is long-wavelength or not), which causes the inelastic event in pristine crystals at 0 K, can be probed very accurately by atomistic calculations [146,154]. In this case, even with ordinary MD, the effect of indentation rate can be shown to be unimportant, as long as the speed of indentation is much slower than the speed of sound.

However, a real specimen may not be pristine crystal prior to indentation, and may contain point defects, voids, inclusions, dislocations, etc. Heterogeneous nucleation [161] (see for example Fig. 10c) may occur, e.g. nucleation of a dislocation near a pre-existing defect [135]; or simply defect propagation [213] if the new defect is of the same type as and connected to the old defect, e.g. when a dislocation segment breaks free of pinning points and starts to expand. Further, at finite temperature, thermal activation can help the system cross the activation barrier, regardless of whether the barrier is that of homogeneous nucleation, heterogeneous nucleation or defect propagation. This will introduce rate dependence to the  $P$ - $h$  response [214,215]. Following the classic harmonic transition-state theory [216,217], the rate of a possible inelastic event can be expressed as  $R = \nu \exp(-Q(\tau)/k_B T)$ , where  $\tau$  is the local stress at the event site (excluding self-stress of the pre-existing defect in the case of heterogeneous nucleation or defect propagation),  $Q$  is the activation free energy,  $k_B T$  is magnitude of thermal fluctuation and  $\nu$  is the trial frequency. Because this is a theoretical platform that the majority of researchers accept in dealing with rate dependences, it is

very important to cast atomistic simulation results in this language.

The stress  $\tau_c$  at which  $Q(\tau_c) = 0$  is called the athermal threshold, which in the case of homogeneous nucleation was proposed to be related to soft phonons [129,152,161,189,192,209,210], since phonon coordinates constitute the complete basis for atomic motion in a perfect crystal. The term  $\Omega(\tau) \equiv -\partial Q/\partial\tau$  is defined as the true activation volume: it has units of volume and is in general a strain-like symmetric tensor.  $\Omega(\tau)$  is an important quantity to access, and the systematic measurement of this parameter by nanoindentation has been performed by Ngan and co-workers [214] and Schuh et al. [215,218]. The reason is because once  $Q(\tau_o)$  and  $\Omega(\tau_o)$  are measured at some reference stress  $\tau_o$ , then the probabilistic rate of this inelastic event occurring at any other stress  $\tau$  can be approximated by a linear expansion  $Q(\tau) \approx Q(\tau_o) - \text{Tr} \Omega(\tau_o)(\tau - \tau_o)$ . In other words, the activation volume is simply the tangent slope of activation energy with respect to the local stress. One must be careful in using the above linearized expansion at  $\tau_o = \tau_c$ , however, because it is a rigorous result that  $\Omega(\tau_c) = 0$  for any system, whether in homogeneous nucleation [154,189], heterogeneous nucleation [161] or defect propagation [213,227]. This is due to the fact that at  $\tau_c$ , the initial minimum and the saddle-point configurations merge.

The timescale challenge for atomistic simulations is therefore to extract  $Q(\tau)$  and  $\Omega(\tau)$  information efficiently and accurately, for microscopic processes that could be rate-limiting under the indenter. Conventional MD is not going to be effective for inelastic events with  $Q(\tau) > 10k_B T$  (0.25 eV if  $T$  is room temperature), because one needs to numerically integrate over at least  $\sim e^{10} = 2 \times 10^4$  vibrational periods to have a reasonable chance of observing one such inelastic event in the simulation. Since numerical stability of the MD time integrator usually requires  $\sim 50$  time steps to integrate over one period of the highest vibrational frequency mode, this means  $\sim 10^6$  time steps to catch one such inelastic event. It would take about 3 days on a reasonably priced personal computer, for the  $10^6$  atom,  $23 \times 23 \times 23$  nm copper cube mentioned above, which is on the borderline of what is acceptable.

Thus, a more “clever” approach needs to be taken, such as hyper-MD [136], dimer dynamics [219] or any of the long-timescale methods currently under active development [220]. The problem is challenging because there are many possible inelastic events for any specific configuration, and perhaps only a small fraction of these are relevant experimentally. Furthermore, the rate-limiting event or saddle-point may change when  $\tau$  is varied or if the configuration has further evolved, in which case we say there is a switch in the rate-limiting mechanism [134].  $\Omega(\tau_o)$  is a good predictor of when this switching might occur [134].

While no one has so far carried out these rate-sensitive calculations with indenters, some relevant work can be noted. To our best knowledge, the first atomistic activation energy calculation involving dislocation was performed by Bulatov et al. [221] on kink nucleation and migration in Si.

Rasmussen, Vegge et al. then studied dislocation cross-slip in fcc Cu [222–225], and Wen and Ngan studied kink nucleation in bcc Fe [226], all using the chain-of-states approach [130–133] first developed in chemical physics. These excellent works established the validity of the atomistic approach to accurately characterize nanomechanical activation processes. It differs from the traditional MD approach of studying defects by time integration, so it is not limited by the atomic vibrational timescale, enabling one to study rare events [136]. Zhu, Li and Yip used the same approach to study crack-tip activations, where the controlling variable is not  $\tau$  but the stress intensity factor  $K$ . They have modeled heterogeneous nucleation of dislocation in front of the crack tip [135], and cleavage crack kink nucleation and propagation in Si [213,227]. There should not be any fundamental difficulty to perform similar calculations under nanoindentation loading. This appears to be the best strategy to address the timescale challenge for atomistic models at this moment.

## 6. In situ observations of nanoindentation

While conventional nanoindentation tests are able to quantitatively measure the mechanical behavior of materials, the discrete deformation mechanisms that contribute to the measured behavior are rarely observed directly. Typically, the mode of deformation during a nanoindentation test is only studied ex post facto, or in situ but by indirect techniques such as Raman spectroscopy [228] or electrical resistivity measurements [229]. Recently, the phenomenological interpretation of nanoindentation tests, and indeed the mechanical behavior of solids at their elastic limit, has been addressed by the experimental technique of in situ nanoindentation in a transmission electron microscope (Fig. 12 shows a typical specimen geometry). This experimental technique has shown direct observations of the nanoindentation-induced deformation behavior in bulk

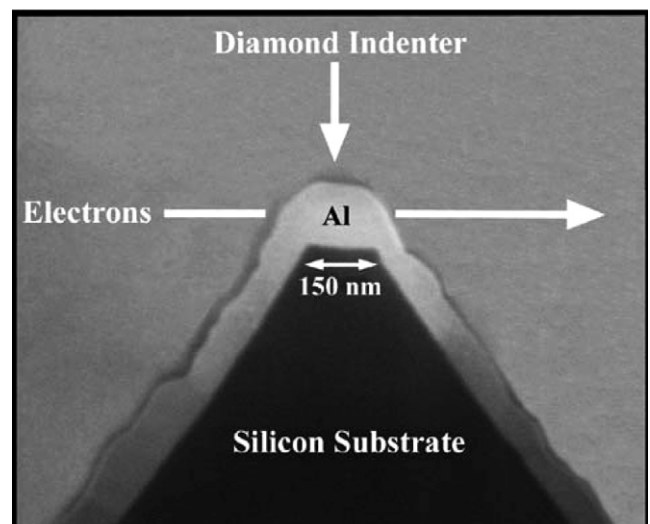


Fig. 12. SEM photograph of an in situ indentation TEM specimen.

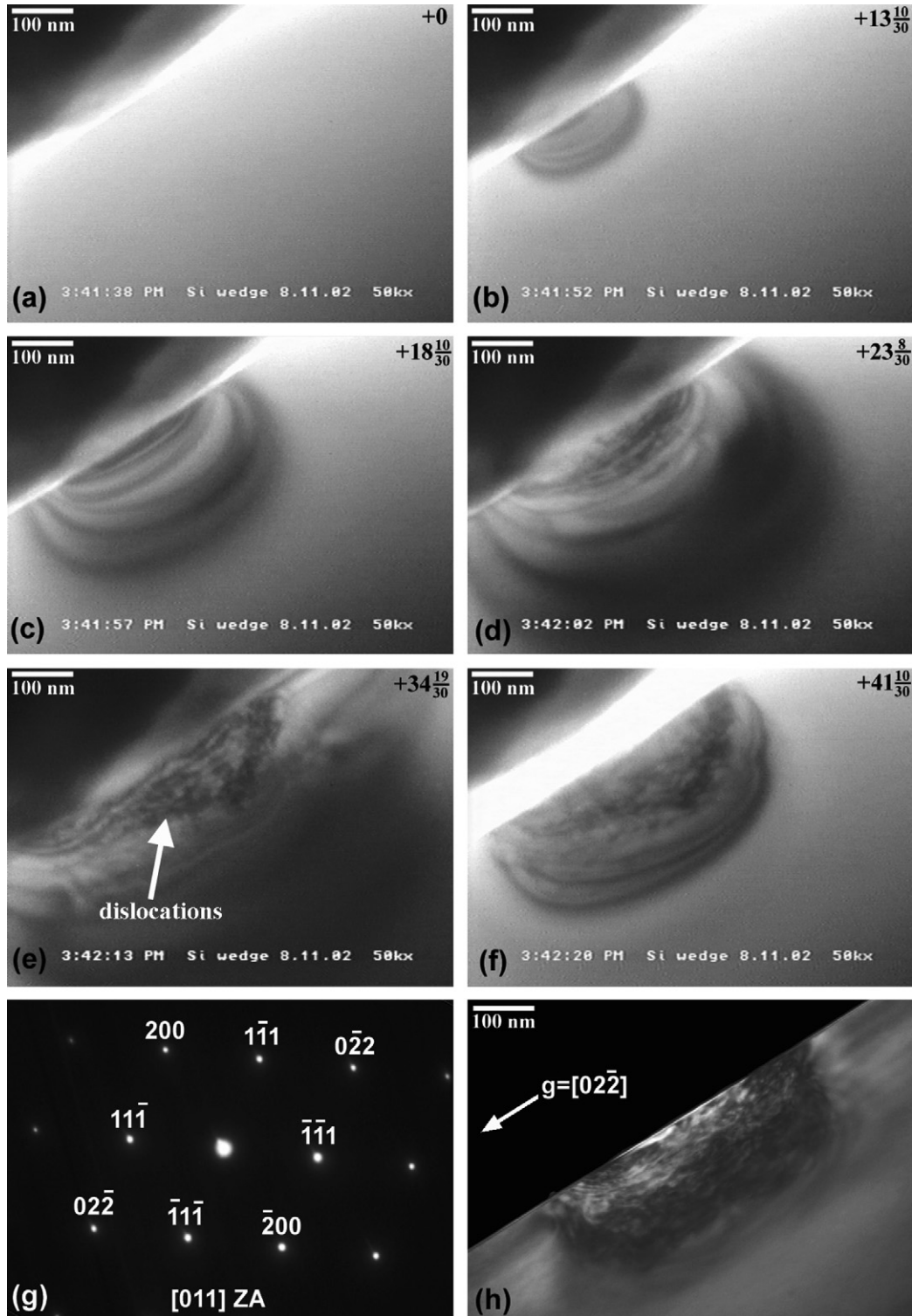


Fig. 13. (a)–(f) Time series taken from a video of an in situ nanoindentation into silicon  $\langle 100 \rangle$ . The diamond indenter is in the top left corner of each frame, and the silicon sample is in the lower right. The time in seconds from the beginning of the indentation is shown in the top right corner of each frame. (a) Prior to indentation the silicon sample is defect free. In (b) and (c) the initial stage of indentation shows elastic strain contours resulting from the pressure applied by the indenter. In (d) and (e) the dislocations can be seen to nucleate, propagate and interact as the indentation proceeds. (f) After a peak depth of 54 nm the indenter is withdrawn and the residual deformed region consists of dislocations and strain contours that are frozen in the sample. (g) A 011 zone axis electron diffraction pattern of the indented region directly after the in situ indentation. With the exception of slight peak broadening, the diffraction pattern is identical to similar patterns taken prior to indentation, showing only single-crystal diamond cubic silicon with no additional phases. The tails seen on the diffraction spots pointing in the  $\langle 200 \rangle$  direction are a geometrical effect due to the wedge geometry, which exhibits a drastic change in thickness over a very short distance. Fig. 7(h) is the same indentation in a  $g = (02\bar{2})$  dark-field condition. Note the continuous surface across the indented region, indicating that the indentation left at least one side of the wedge intact.

materials [230,231] and thin films [232–235]. Here we focus our comments on two important engineering materials that serve as model metallic and ceramic systems, Si and Al.

### 6.1. Case study: silicon

Over 50 years of research on dislocation behavior in Si supports the conclusion that dislocations do not generally move during conventional mechanical testing at temperatures below 450 °C [236,237]. Under large-deformation conditions such as indentation loading, where localized stresses can approach the theoretical shear strength of the material, dislocation structures have been observed in Si. Traditionally, these are thought to result from either block slip [238,239], or phase transformations [240–242], rather than the nucleation and propagation mechanisms associated with conventional dislocation plasticity. However, recent results have shown evidence of room temperature dislocation plasticity in Si in the absence of phase transformations through post-mortem transmission electron microscopy (TEM) of shallow indentations [243].

Direct nanoscale observations of deformation mechanisms during the earliest stages of indentation in silicon were reported using the technique of in situ nanoindentation in a transmission electron microscope [244]. The in situ experiments were performed on  $\langle 100 \rangle$  n-type single-crystal silicon samples that were fabricated lithographically in the shape of a wedge. The wedge geometry provides electron transparency as well as mechanical stability. Indentations were performed on two different wedge geometries, where the wedge was either terminated by a flat plateau  $\sim 150$  nm in width, or sharpened to a plateau width of approximately  $\sim 20$  nm.

In situ nanoindentation experiments were performed on the silicon wedge samples to peak depths ranging between 50 and 200 nm. Indentations to depths greater than 200 nm were not performed in situ due to the inherent limitations in electron transparency of the wedge geometry. During in situ indentation the deformation is observed and recorded in real time, and diffraction patterns are taken directly after unloading. It was found that plastic deformation proceeds through dislocation nucleation and propagation in the diamond cubic lattice. Fig. 13 shows a series of images taken during an indentation into the “blunt” geometry, which had a plateau of  $\sim 150$  nm at the top of the wedge. Fig. 13(a) shows the defect-free sample prior to indentation. Fig. 13(b) and (c) shows the evolution of elastic strain contours as the indenter presses into the sample – no evidence of plastic deformation is seen at this point. The elastic strain contours reveal the shape of the stress distribution in the sample (these are essentially the contours of principal stress). Fig. 13(d) and (e) clearly shows the nucleation and propagation of dislocations from the surface as deformation proceeds. This particular indentation was taken to a peak depth of 54 nm, resulting in the plastic zone shown in Fig. 13(f). The post-indentation selected area diffraction pattern of the indented region is shown in

Fig. 13(g). Due to the high density of dislocations after indentation, a slight broadening of the diffraction spots is observed. The broadening of diffraction spots is an expected consequence of a high density of dislocations created on multiple slip planes [245]. However, no additional diffraction spots or rings are present after indentation as compared to diffraction patterns taken prior to indentation. This indicates that no additional phases (crystalline or amorphous) have formed. Fig. 13(h) is a dark-field condition using the  $(0\bar{2}2)$  diffracted beam, showing that at least one edge of the plateau is still continuous across the indented region.

In the case of deeper indentations, significant metal-like extrusions were also formed during indentation. These large extrusions are shown in Fig. 14(a), a post-indentation TEM micrograph of a 220 nm deep indentation with the corresponding diffraction pattern. This metal-like deformation can clearly be seen in Fig. 14(b), which is a plan view micrograph of the indent shown in Fig. 14(a), taken with a field emission scanning electron microscope. Previous

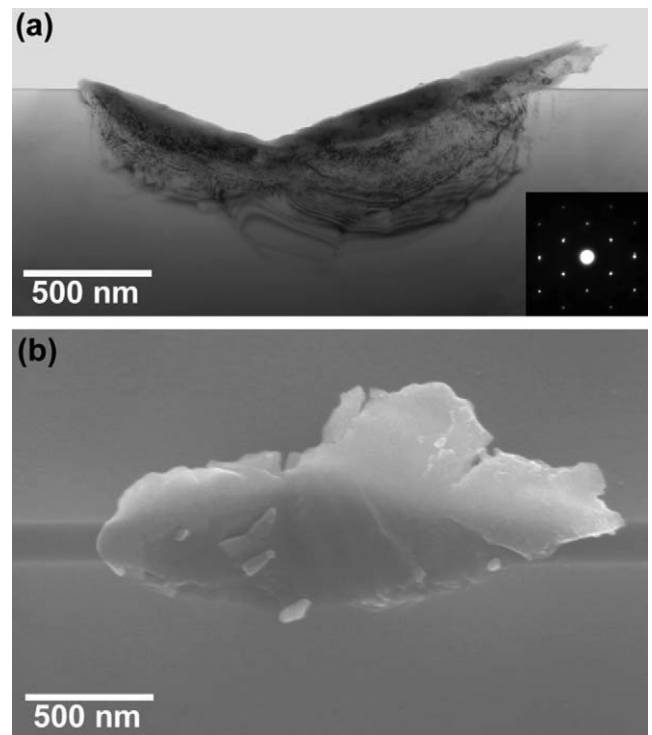


Fig. 14. (a) Bright-field TEM micrograph of an in situ indentation into  $\langle 100 \rangle$  silicon that was taken to a depth of 220 nm. The image was taken in a kinematic condition in order to show the undeformed region surrounding the indented volume, which was heavily deformed through dislocation plasticity. The 110 zone axis electron diffraction pattern inset was taken after indentation and shows only the presence of the diamond cubic phase of silicon. This diffraction pattern is identical to diffraction patterns taken before indentation, except for a slight broadening of the diffraction spots due to the heavily dislocated region of the indentation. (b) A plan-view scanning electron micrograph of the same indentation. Relatively large, metal-like extrusions can be seen surrounding the indentation. These extrusions can also be seen above the indented volume in (a), and as shown by the inset diffraction pattern are extrusions of single-crystal diamond cubic silicon.

studies [246–248], have also described metal-like extrusions resulting from indentation into Si. However, in all previous experimental cases these extrusions were attributed to the flow of a transformed metallic phase (such as  $\beta$ -Sn or bcc R8). As shown in Fig. 14(a), the diffraction pattern taken after the indentation indicates that the extruded volume is entirely single-crystal diamond cubic silicon in the same orientation as the rest of the sample. Since dislocations are more easily nucleated heterogeneously at a surface as opposed to homogeneously in the bulk, it seems that dislocation plasticity can completely accommodate the deformation imposed by the indenter in the in situ wedge geometry (to the indentation depths observed here). Thus the hydrostatic pressures required to trigger the phase transformations are never achieved, and dislocation plasticity is the only mode of deformation observed. This is in contrast to the state of stress under conventional nanoindentation or cutting, which ostensibly promotes such transformation. Further comment on this, in the context of ductile machining of semiconductors, is provided in Section 7.

## 6.2. Case study: Al thin films

The interpretation of conventional nanoindentation data is not always clear. For example, since most metals form native oxides, yielding under the nanoindenter may be governed by fracture of the oxide film rather than the onset of plastic deformation in the material itself [107]. It is difficult to resolve these mechanisms *ex situ* since the mechanisms associated with yielding are only indirectly elucidated from quantitative load vs. displacement behavior. Thus, the most significant advantage from performing in situ nanoindentation inside a transmission electron microscope is the ability to record the deformation mechanisms in real time, avoiding the possibility of artifacts from post-indentation sample preparation. However, since the Peierls barrier in Al is extremely low, and consequently the dislocation velocity is very fast, the typical video sampling rate of 30 frames/s is too slow to capture the movement of the individual dislocations. Hence, each video image captured during the in situ experiments performed to date is essentially a quasi-static image of the equilibrium configuration of defects. Fig. 15 illustrates this point by showing a series of six images taken from a video during an in situ nanoindentation experiment. In Fig. 15(a), the diamond is approaching an Al grain that is approximately 400 nm in diameter. Fig. 15(b) and (c) shows images of the evolution of the induced stress contours during the initial stage of indentation, and corresponds to purely elastic deformation in the absence of any pre-existing dislocations that could cause plasticity. Fig. 15(d) shows the first indication of plastic deformation, in which dislocations are nucleated. Fig. 15(c) and (d) shows consecutive frames of the video, and are 1/30th s apart. As can be seen, the exact location of the nucleation event is not discernible, since the evolution of the dislocation configuration has already

proceeded beyond the point at which that might be possible. Fig. 15(e) and (f) shows the large increase in dislocation density achieved as deformation proceeds, and dislocations tangle and multiply.

In polycrystalline metals with relatively large grain sizes (e.g.  $>1\ \mu\text{m}$ ), grain boundaries are thought to behave primarily as barriers to dislocation motion. Consequently, a typical method for increasing the hardness of a metal is to change the composition or processing of the material in order to decrease the average grain size, thus increasing the total area of grain boundaries and increasing the barriers to dislocation motion. This basic premise of microstructure–property relations in metallurgy is known as Hall–Petch behavior, since the first studies to relate grain size with the strength of a material were performed by Hall [249] and Petch [250] in the early 1950s.

There are other known mechanisms by which grain boundaries can influence the mechanical behavior of a polycrystalline metal. Li [251] described an alternate role for grain boundaries in 1963, when he first proposed that grain boundaries be thought of as sources for dislocations rather than only as barriers to their motion. Indeed, recent reports using computational studies of nanoindentation have shown that relatively easier dislocation nucleation at grain boundaries can serve to lower the load at which plasticity is initiated [158].

As grain size decreases, the volume of the material associated with grain boundaries increases dramatically. For a given indenter size, the interaction of the grain boundaries increases as the grain size decreases. Thus, it should not be surprising that the deformation behavior associated with increased grain boundary interaction might involve mechanistic changes. These mechanistic changes might include grain boundary sliding [252,253], dislocation nucleation from the grain boundary [158] or even grain boundary movement. This final mechanism, grain boundary movement, has been observed in further macroscopic experiments, but is typically not mentioned as being relevant to small-scale deformation. Winning et al. [254] described the motion of Al tilt boundaries under imposed external stresses, and suggested that the movement of the grain boundaries was achieved through the movement of dislocations that comprised the structure of the boundaries. Merkle and Thompson [255] ascribed the motion of grain boundaries in Au to a more localized phenomenon – the rearrangement of groups of atoms near a grain boundary leading to incorporation into a growing grain. Whether the grain boundary motion is accomplished through coordinated dislocation motion or atomic rearrangement, there exists a driving force for a grain to grow or shrink under an inhomogeneous external stress. The stresses imposed by a nanoindenter are inhomogeneous [1], and can be expected to provide a significant driving force for the movement of grain boundaries. In fact, the movement of grain boundaries during in situ nanoindentation was observed to be considerable in Al grains under  $\sim 400\ \text{nm}$  in width.

Figs. 16 and 17 show a dramatic example of grain boundary movement, where the size of the indentation contact area is large compared to the size of the grain. Fig. 16 includes a series of four images extracted from the videotape record of an in situ nanoindentation of a small grain approximately 150 nm in width that had formed at the cusp of a grain boundary between three larger grains. In Fig. 16(a), the indenter is approaching the small grain from the upper left corner of the video frame. Starting at Fig. 16(b) and ending at Fig. 16(d), the small grain can be observed to shrink dramatically over a very short time (0.2 s elapsed between these three frames). By comparing the pictures taken before and after indentations (Fig. 17), it can be seen that the two larger grains laterally surrounding the small grain in the cusp grew at the expense of the shrinking grain. Fig. 17(a) and (c) shows bright-field

images before and after the indentation, respectively, showing the change in grain size of all of the grains. Fig. 17(b) and (d) are dark field images of the small grain in the cusp taken before and after the indentation, respectively, clearly showing the shrinkage of the small grain after the indentation. It can be noted from the consistent contrast in the small grain before and after indentation that the small grain did not simply change its shape, and that the volume of this grain was not conserved. If the volume of this grain had been conserved, then the thickness of the grain in the direction of the electron beam would have increased, resulting in a significant change in contrast as compared to the surrounding grains, which was not observed.

The motion of grain boundaries can be effectively suppressed by the addition of a solute to the Al films, and in situ nanoindentation experiments reported previously

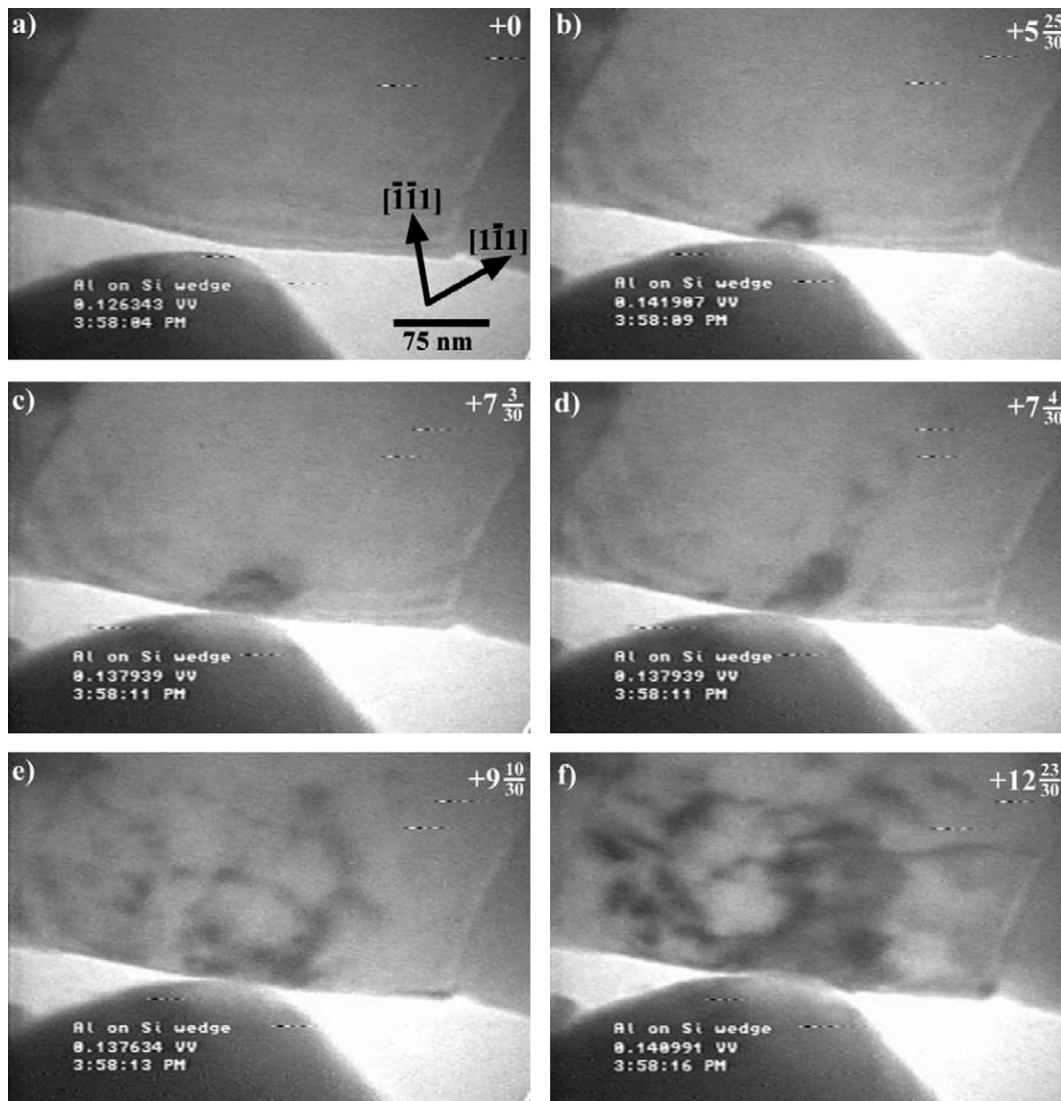


Fig. 15. Time series of an Al grain showing the evolution of plastic deformation during an in situ nanoindentation. The time elapsed from image (a) is given in seconds in the upper right corner of each frame. Images (b) and (c) correspond to elastic deformation only. In image (d) the nucleation of dislocations can be seen. (e) and (f) is characteristic of the resulting plastic deformation during deeper penetration and the pile-up of the dislocations at the grain boundaries and the substrate–film interface.

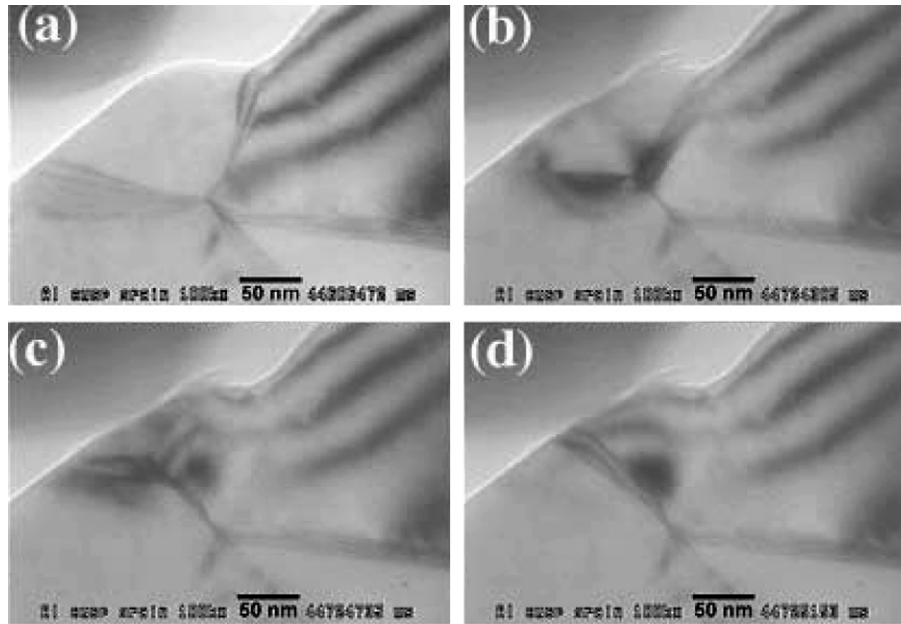


Fig. 16. A series of images extracted from a videotape record showing the stress-induced grain growth during an in situ nanoindentation on submicron-grained aluminum: (a) before indentation the indenter approaches from the upper-left corner, (b) the indenter makes contact with a small grain in the cusp of three larger grains. (c) The small grain in the cusp starts to shrink and is left as a small film (d) between the neighboring grains.

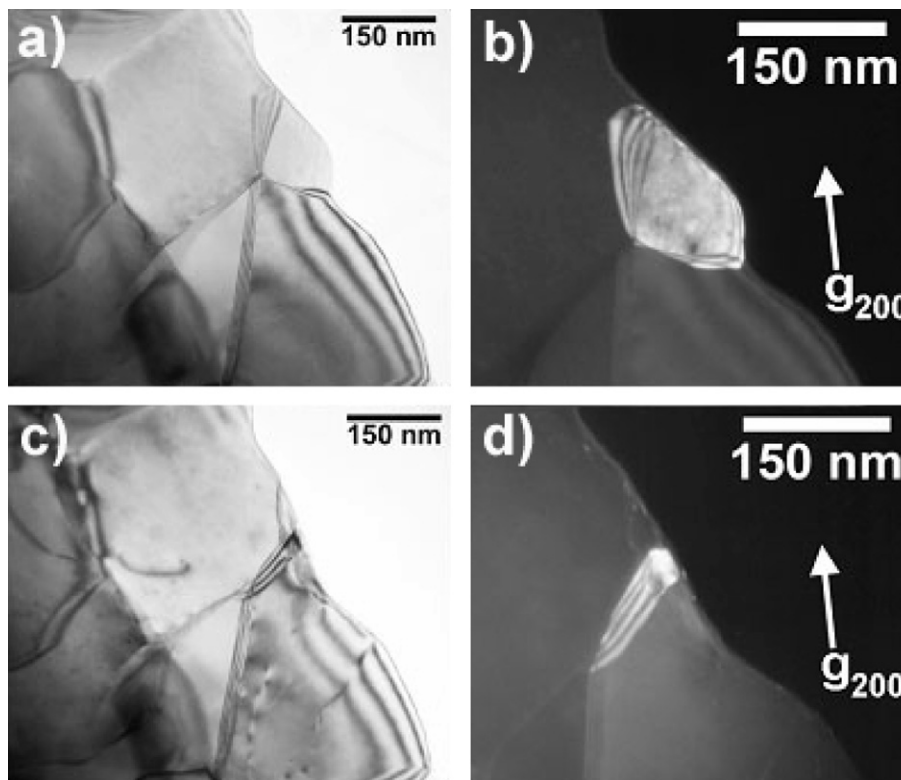


Fig. 17. Still images from the indentation shown in Fig. 15. (a) Bright-field image before the indentation. (b) Dark-field image of the middle small grain before the indentation. (c) Bright-field image after the indentation. (d) Dark-field image of the middle small grain after the indentation.

showed that the addition of as little as 1.8 wt.% Mg to the same Al films pinned the high-angle grain boundaries [256]. Nevertheless, the observation of dramatic grain boundary movement in the pure Al films suggests that grain bound-

ary motion is a significant mechanism of deformation during nanoindentation, and in fact might play a large role in the softening of materials with sub-micron grain sizes. For example, similar grain boundary motion was found in

nanocrystalline Al films with a grain size on the order of 20 nm [233]. Since, given Le Chatelier's principle, all spontaneous processes that happen under load contribute to the relaxation of the load, it is very likely that coalescence plays a significant role in the extraordinary mechanical behavior of nanocrystalline materials.

### 6.3. Future directions

In prior work [232,257], attempts have been made to correlate load–displacement behavior with real-time images of the deformation response during in situ nanoindentation in a transmission electron microscope. However, these attempts have relied on ex post facto determination of indenter displacement from sequential TEM images as well as indirect correlations between voltages applied to the piezoceramic actuator and measurements of known bending moments. This approach suffers from substantial uncertainties caused by nonlinearities in the piezoceramic response, resulting in inexact data with low temporal and load resolution. A recent collaboration between the National Center for Electron Microscopy (NCEM) at the Lawrence Berkeley National Laboratory and Hysitron, Inc., has resulted in a new in situ TEM nanoindentation holder design that includes a capacitive load sensor for quantitative force and displacement measurement during in situ indentations [258]. The quantitative holder has a force resolution of  $\sim 0.2 \mu\text{N}$  and a displacement resolution of  $\sim 0.5 \text{ nm}$ . By correlating the force–displacement response of the material with direct images of the microstructural response of a material in real time, it is possible to study the initial stages of plasticity in metals [259,260], semiconductors [261] and even individual nanoparticles [262]. In conclusion, the experimental technique of in situ nanoindentation in a transmission electron microscope has been shown to provide a unique capability for investigating the nanomechanical behavior of small solid volumes. This capability is essential to fully understanding the mechanisms associated with indentation phenomena and the fundamental deformation behavior of materials.

## 7. Non-traditional uses for indentation

From the above sections, it can be summarized that much effort has been expended to understand the nature of hardness. From a continuum perspective, it comprises the bulk elastic and plastic behavior of a metallic material, or perhaps the combined response of layers and/or material inclusions. On a much smaller scale, discrete dislocation activity is the dominant physical phenomenon occurring under nanoscale contact. However, although the fundamentals of inelastic deformation in metallic materials are important, to say the least, the flexibility of indentation as a material probe would be short-changed if discussions were restricted to this. Thus, in this section we review emerging uses for this tool in other materials systems, in which elastic and inelastic deformation are not governed

by the same mechanisms as those in bulk metallic materials, and for which traditional mechanical testing would be extremely difficult. What does hardness mean in these systems? By posing (and addressing) this question, important nanostructural, microscopic and even physiological issues may be explored. In other cases, researchers are not concerned with hardness, but have capitalized upon the ultra-precise control of force, displacement and probe location offered by modern indentation systems. Specific activities are reviewed briefly here, with an extended discussion to include macro- and microindentation as well.

### 7.1. Mechanics of nanotubes

The nigh-incredible mechanical properties of carbon nanotubes are now well known in the materials literature (e.g. Refs. [263,264]). However, due to their size, shape and growth method, systematic tensile testing of these structures, or nanotubes in general, is rather difficult. A number of researchers have addressed this problem using a variety of methods [265–273]. For one approach, an indenter tip is used, not to determine hardness per se, but rather for its precise control of normal force and displacement. In one set of experiments, nanotubes were grown normal to a substrate, and bent as a cantilever (using an AFM tip) to determine bending stiffness [266]. Similar experiments have involved isolating single nanotubes and positioning them over gaps on a nanoporous substrate, allowing precise three-point bending tests [265]. While these studies are innovative, they require isolation of nanotubes, whereas these materials are often grown in entangled bunches [264] or vertically aligned “forests” (Fig. 18(a)) [269]. Accordingly, nanoindentation and related analyses have been performed on these latter configurations [269], and it is necessary to take into account the inherently anisotropic nature of the specimens, and the dominant contribution of tube bending to the indentation response (Fig. 18(b)). Results correlated well with atomic simulations [270] and other experimental approaches. Finally, indentation experiments have been carried out to determine the effective buckling load of these structures in pure compression [271]. A reasonable and necessary future direction for indentation-based work on nanotubes would be the extension of indentation to study interaction forces between tubes, which would be critical for “scaling up” from single tubes into ropes or cables [273,274].

### 7.2. Soft biomaterials

The mechanical behavior of soft tissues is quite different from that of harder biomaterials (i.e. bone, cartilage, which can be readily nanoindented – see e.g. Refs. [275–278]) as one must often consider viscous effects, as well as large deformations. In addition, a number of biological systems, including eyes, brain, viscera and lungs, have geometries that do not lend themselves to traditional mechanical testing and also may not be machined or cut to produce

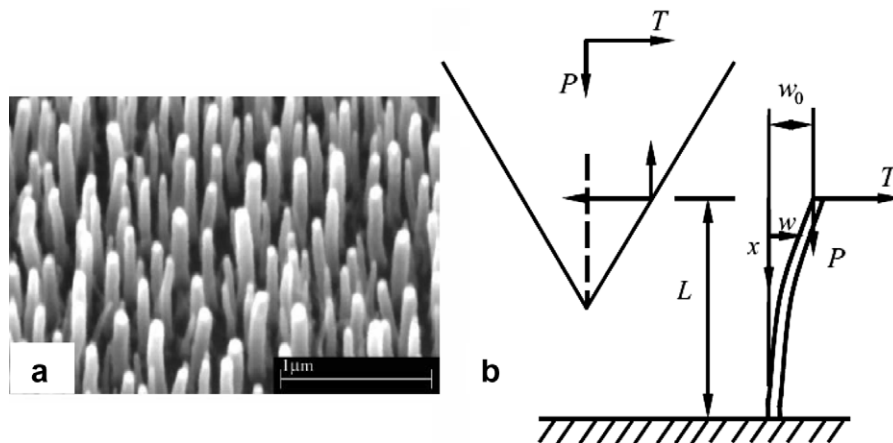


Fig. 18. (a) SEM photo of a nanotube “forest” on a substrate. (b) Free-body diagram used to analyze nanoindentation experiments on vertical arrays of nanotubes [269].

convenient samples. For these, indentation can serve as a powerful probe of mechanics, function and disease. In the field of respiratory physiology, indentation has been used to determine the elastic modulus of lungs at different pressures [279]. However, on a smaller scale, microindentation experiments have been performed on the pleural surfaces of the lung and chest wall to simulate elastohydrodynamic deformation during breathing (Fig. 19(a)) [280]. Currently, hardness tests are performed on lungs, not to extract any properties in the engineering sense, but as an

indicator of atelectasis (partial collapse) [281,282]. Such work can be termed “translational physiology”, i.e. research results can be directly communicated to surgeons or anesthesiologists for rapid implementation. In other systems, quantitative tactile detection and characterization of breast tumors by mechanical palpation is being pursued. The measurement relies on the spatial differences in response by recourse to multi-pronged indenters, and is based on the increased stiffness of tumors relative to healthy tissue [283]. In the same spirit, correlation of extent

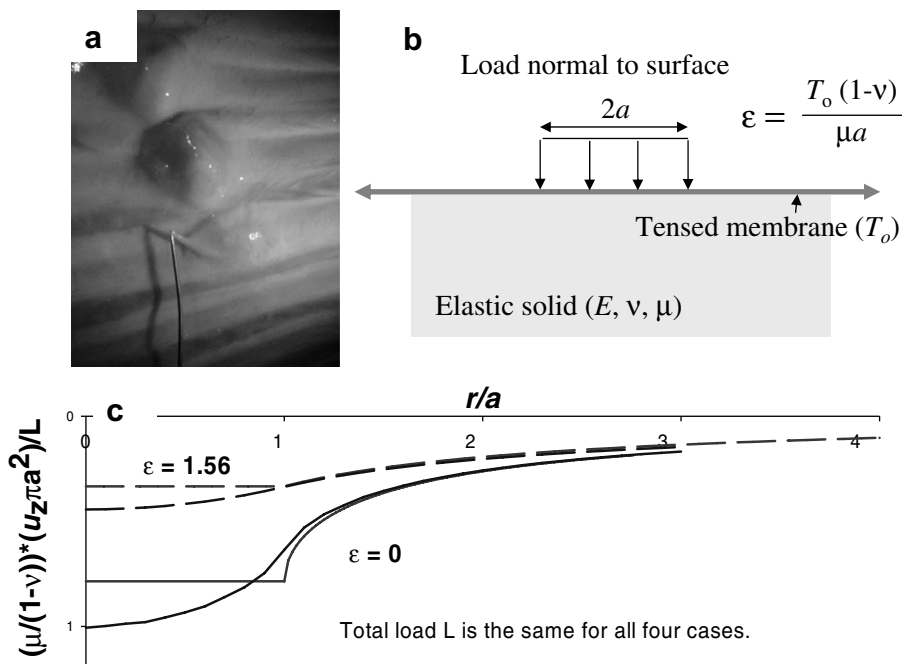


Fig. 19. (a) Parietal pleural surface of a sheep ribcage, in which a thin membrane covers ribs and intercostal muscles. The lung slides against this during breathing. Indentation experiments were performed to understand the role of mechanical properties in pulmonary lubrication. (Note that bumps are an artifact of rib fracture, and are not physiological.) (b) For proper analysis, the problem of indentation of a tensed membrane on an elastic material was addressed, for a circle of constant pressure [279] or a rigid, flat punch [280]. (c) Selected results show the effect of the membrane on normalized indentation deformation under (smooth lines) constant pressure and (kinked line) flat punch. Increasing values of  $\epsilon$  indicate greater influence of membrane on results.

of cirrhotic fibrosis in the liver and “hardness” measured via a tactile sensor is being explored, to guide decision-making before possible liver resection [284,285].

In addition, tactile interaction with our environment depends on physical contact with outside objects, and transduction of pressure to electrical nervous signals – in short, a complex indentation problem. The science of touch, or haptics, is critical for a number of engineering and bioengineering fields, including virtual environments, robotics, prosthetics and physical rehabilitation [286]. In essence, the contact underneath a fingertip can be addressed in the context of indentation, and similar approaches can be used to analyze, for example, local pressures, friction and deformation [287,288].

For the above investigations, robust knowledge and/or appreciation of the fields underneath the indenter tip are critical for success. Also, for these materials, the simplifying assumptions often made in nascent indentation experiments (e.g. linear elasticity) may not be appropriate. For example, in the cases of lung indentation, the authors necessarily solved the problem of punch indentation of an elastic half-space, covered with a tensed membrane (Fig. 19(b) and (c)) [279,280]. Such an approach will probably be found necessary in future studies involving skin, which is under tension. In haptics, a great deal of effort is being expended to develop appropriate viscoelastic and large deformation models of fingertips. It is likely that for significant progress in this direction, contact mechanics will become a necessary component of the bioengineer’s toolbox.

### 7.3. Nanomachining, manufacturing and combinatorial studies

Many of the continuum-based studies of indentation are carried out with the goal of gaining knowledge about mechanical behavior under some other form of loading. For more complex materials systems and at small size scales, it becomes increasingly clear that mechanical response is not only dependent upon magnitude of load, but on how it is applied. Thus, it is encouraging to report that there are a number of activities in the literature that progress beyond fundamental mechanics of materials, and pursue correlations between nanoindentation, and its close relative nanotribology, in engineering systems. A few examples are highlighted here. In the semiconductor industry, wafer fabrication from ingot form is a multistep process with extremely high tolerances. The shift to larger wafers has necessitated the use of different cutting mechanisms, e.g. wiresaw slicing (Fig. 20(a)) [289]. In addition, lapping and polishing techniques must be carried out so as to minimize of warpage. In all these procedures, the wafer material is subjected to a lubricating flow of hard particles in a suspending medium. This is analogous to repeated loading under a small load/tip. Thus, in this case, nanoindentation studies can provide a direct indicator of material removal mechanisms, or a predictor of variations

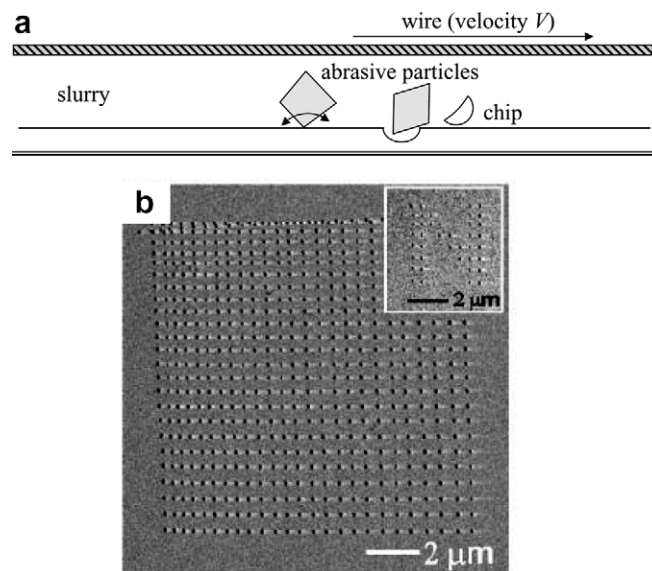


Fig. 20. (Top) Schematic of rolling-indenting mechanism of abrasion during wiresaw slicing [289]. Indentation experiments, performed in conjunction with manufacturing experiments, may be a powerful tool for controlling the process. (Bottom) Results of mechanical lithography, in which PMMA was nanoimprinted (with an AFM tip) in an array, and the resulting deformed pattern was used for deposition of Au [305].

in the machining process. Although Si is a well-characterized material, other semiconductors, such as lithium niobate, have not been explored as systematically [119]. In this particular material, the highly asymmetric crystal group can lead to interesting tribological behavior, e.g. different rates of polishing on parallel faces. The reasons for this, in the context of subsurface inelasticity and fracture under nanoscale contact, are being studied [119]. Another strong connection between contact mechanics and manufacturing is in the field of ductile machining of brittle materials such as Si, on the micro- or nanoscale [290–295]. One of the cornerstones of this is the observation and explanation of high-pressure, high-shear phase transformations that occur under localized contact [240,296–300]. Such transformations are ostensibly manifested (in Si) as “pop-outs”, that is to say, rapid changes in displacement upon nanoindentation unloading [301,302].

In other semiconductor systems, the concept of nanoimprint lithography was first introduced in 1994 as a means to pattern a surface to submicron dimensions using non-chemical methods [303]. The concept involves the pressing of a rigid die pattern into a layer of photoresist, and then removing the subsequently compressed areas via anisotropic etching. Although proving quite successful, limiting issues for this technique involve die preparation and lateral precision [303,304]. As a variation on this, some researchers are employing nanoindentation to preferentially expose sapphire, by probing a thin PMMA cover layer with a Berkovich tip in an  $x$ - $y$  array (Fig. 20(b)). The resulting patterned structure is sputtered with Au, and the underlying PMMA layer is rinsed away with a solvent, leaving an array of Au nanodots on the surface. These dots serve as

a catalyst for the preferential growth of ZnO nanowires [305].

Finally, although one of the attractive features of instrumented nanoindentation is the potentially high throughput of experiments (i.e. a large number of mechanical tests in a short time), this has not been exploited until recently. In a combinatorial materials study, Tweedie et al. indented a triplicate array of over 540 polymer microdot samples, from different combinations of constituent monomers, over a 24 h period [306]. Significant differences in indentation modulus between samples with minor changes in composition were interpreted as (unpredicted) phase changes, illustrating that mechanical probing can be a powerful supplement in the synthesis of soft materials. A similar approach for metallic alloys can be found in Ref. [307].

## 8. Concluding remarks

The experimental flexibility of indentation has provided insights into the fundamental structure and deformation processes of materials across a range of size scales and disciplines. Much of this has been due to (i) concentrated studies of the concept of hardness, and what this value truly represents, and (ii) greatly enhanced computational power. However, it has also been shown that a number of opportunities still exist for the implementation of this technique in emerging systems, and creative modeling coupled with investigations carried out in conjunction with other functional considerations may provide great benefit to the scientific, engineering and biomedical communities.

## Acknowledgements

A.G. was supported through NSF CAREER award CMS 0449268. N.C. acknowledges support of MTEC. M.D. acknowledges the financial support of the Defense University Research Initiative on Nano Technology (DURINT) which is funded at MIT by the ONR under grant N00014-01-1-0808. J.L. is supported by NSF DMR-0502711, AFOSR FA9550-05-1-0026, ONR N00014-05-1-0504, and National Energy Technology Laboratory DE-AM26-04NT41817. A.M.M. was supported by the Director, Office of Science, Office of Basic Energy Sciences, of the US Department of Energy under Contract No. DE-AC02-05CH11231. Y.L.S. acknowledges support from the Air Force Office of Scientific Research.

## References

- [1] Johnson KL. Contact mechanics. Cambridge: Cambridge University Press; 1987.
- [2] Alcalá J, Giannakopoulos AE, Suresh S. *J Mater Res* 1998;13(5):1390–400.
- [3] Ahn JH, Kwon D. *J Mater Res* 2001;16(11):3170–8.
- [4] Cao YP, Lu H. *Acta Mater* 2004;52(13):4023–32.
- [5] Lee H, Lee JH, Pharr GM. *J Mech Phys Solids* 2005;53(9):2037–69.
- [6] Zhao MH, Ogasawara N, Chiba N, Chen X. *Acta Mater* 2006;54(1):23–32.

- [7] Tabor D. Hardness of metals. Oxford: Clarendon Press; 1951.
- [8] Dao M, Chollacoop N, Van Vliet KJ, Venkatesh TA, Suresh S. *Acta Mater* 2001;49(19):3899–918.
- [9] Cheng YT, Cheng CM. *Mater Sci Eng R* 2004;44(4–5):91–149.
- [10] Fischer-Cripps AC. *Surf Coat Technol* 2006;200(14–15):4153–65.
- [11] Bull SJ. *J Phys D – Appl Phys* 2005;38(24):R393–413.
- [12] VanLandingham MR. *J Res Natl Inst Stand Technol* 2003;108(4):249–65.
- [13] Oliver WC, Pharr GM. *J Mater Res* 2004;19(1):3–20.
- [14] Bucaille JL, Stauss S, Felder E, Michler J. *Acta Mater* 2003;51(6):1663–78.
- [15] Chollacoop N, Dao M, Suresh S. *Acta Mater* 2003;51(13):3713–29.
- [16] Giannakopoulos AE, Suresh S. *Scr Mater* 1999;40(10):1191–8.
- [17] Giannakopoulos AE, Suresh S. *Int J Solids Struct* 1997;34(19):2393–428.
- [18] Suresh S, Giannakopoulos AE, Alcalá J. *Acta Mater* 1997;45(4):1307–21.
- [19] Nakamura T, Wang T, Sampath S. *Acta Mater* 2000;48(17):4293–306.
- [20] Aizikovitch SM, Alexandrov VM, Kalker JJ, Krenev LI, Trubchik IS. *Int J Solids Struct* 2002;39(10):2745–72.
- [21] Gu Y, Nakamura T, Prchlik L, Sampath S, Wallace J. *Mater Sci Eng A* 2003;345(1–2):223–33.
- [22] Fischer-Cripps AC. *Surf Coat Technol* 2003;168(2–3):136–41.
- [23] Guler MA, Erdogan F. *Mech Mater* 2006;38(7):633–47.
- [24] Suresh S, Giannakopoulos AE. *Acta Mater* 1998;46(16):5755–67.
- [25] Carlsson S, Larsson PL. *Acta Mater* 2001;49(12):2193–203.
- [26] Carlsson S, Larsson PL. *Acta Mater* 2001;49(12):2179–91.
- [27] Lee YH, Kwon D. *Acta Mater* 2004;52(6):1555–63.
- [28] Chen X, Yan J, Karlsson AM. *Mater Sci Eng A* 2006;416(1–2):139–49.
- [29] Rar A, Pharr GM, Oliver WC, Karapetian E, Kalinin SV. *J Mater Res* 2006;21(3):552–6.
- [30] Giannakopoulos AE, Suresh S. *Acta Mater* 1999;47(7):2153–64.
- [31] Sridhar S, Giannakopoulos AE, Suresh S, Ramamurty U. *J Appl Phys* 1999;85(1):380–7.
- [32] Sridhar S, Giannakopoulos AE, Suresh S. *J Appl Phys* 2000;87(12):8451–6.
- [33] Ramamurty U, Sridhar S, Giannakopoulos AE, Suresh S. *Acta Mater* 1999;47(8):2417–30.
- [34] Cheng YT. *Philos Mag Lett* 2001;81(1):9–16.
- [35] Takagi H, Dao M, Fujiwara M, Otsuka M. *Philos Mag* 2003;83(35):3959–76.
- [36] Fischer-Cripps AC. *Mater Sci Eng A* 2004;385(1–2):74–82.
- [37] Oliver WC, Pharr GM. *J Mater Res* 1992;7(6):1564–83.
- [38] Doerner MF, Nix WD. *J Mater Res* 1986;1(4):601–9.
- [39] Giannakopoulos AE, Larsson PL, Vestergaard R. *Int J Solids Struct* 1994;31(19):2679–708.
- [40] Larsson PL, Giannakopoulos AE, Soderlund E, Rowcliffe DJ, Vestergaard R. *Int J Solids Struct* 1996;33(2):221.
- [41] Venkatesh TA, Van Vliet KJ, Giannakopoulos AE, Suresh S. *Scr Mater* 2000;42(9):833–9.
- [42] Barenblatt GI. Scaling self-similarity and intermediate asymptotics. Cambridge: Cambridge University Press; 1996.
- [43] Larsson PL. *Int J Mech Sci* 2001;43(4):895–920.
- [44] Cao YP, Qian XQ, Lu J, Yao ZH. *J Mater Res* 2005;20(5):1194–206.
- [45] Ogasawara N, Chiba N, Chen X. *Scr Mater* 2006;54(1):65–70.
- [46] Ogasawara N, Chiba N, Chen X. *J Mater Res* 2005;20(8):2225–34.
- [47] Muliana A, Steward R, Haj-Ali RM, Saxena A. *Metall Mater Trans A* 2002;33(7):1939–47.
- [48] Huber N, Nix WD, Gao H. *Proc R Soc London A* 2002;458(2023):1593–620.
- [49] Huber N, Tsagrakis I, Tsakmakis C. *Int J Solids Struct* 2000;37(44):6499–516.
- [50] Wang LG, Ganor M, Rokhlin SI. *J Mater Res* 2005;20(4):987–1001.
- [51] Futakawa M, Wakui T, Tanabe Y, Ioka I. *J Mater Res* 2001;16(8):2283–92.
- [52] Swaddiwudhipong S, Tho KK, Liu ZS, Zeng K. *Int J Solids Struct* 2005;42(1):69–83.

- [53] Cao YP, Lu J. *Acta Mater* 2004;52(5):1143–53.
- [54] Dugdale DS. *J Mech Phys Solids* 1954;2:265.
- [55] Dugdale DS. *J Mech Phys Solids* 1955;3:206.
- [56] Atkins AG, Tabor D. *J Mech Phys Solids* 1965;13:149.
- [57] Wang LG, Rokhlin SI. *Int J Solids Struct* 2005;42(13):3807–32.
- [58] Choi Y, Van Vliet KJ, Li J, Suresh S. *J Appl Phys* 2003;94:6050–8.
- [59] Mann AB, Cammarata RC, Nastasi MA (Eds). *J. Mater Res* 1999;14(6):2195–350.
- [60] Zeng K, Chen Z, Dao M, Ramamurty U, Zhang Y-W (Eds). *Mater Sci Eng A* 2006;423(1–2):1–358.
- [61] Matthews A, Marchev K, Patscheider J, Pauleau Y (Eds). *Thin Solid Films* 2004;447–448:1–707.
- [62] Chaudhri MM, Lim YY (Eds). *Philos Mag A* 2002;82:1807–2237.
- [63] Cheng YT, Page T, Pharr GM, Swain MV, Wahl KJ (Eds). *J Mater Res* 2004;19:1.
- [64] Spaepen F. *Acta Mater* 2000;48:31–42.
- [65] Misra A, Kung H. *Adv Eng Mater* 2001;3:217–22.
- [66] Misra A, Hirth JP, Kung H. *Philos Mag A* 2002;82:2935–51.
- [67] Huang HB, Yu DYW, Verdier M, Spaepen F. *Int J Fract* 2003;119:359–64.
- [68] Barshilia HC, Jain A, Rajam KS. *Vacuum* 2003;72(3):241–8.
- [69] Henager Jr CH, Hoagland RG. *Scr Mater* 2004;50:701–5.
- [70] Misra A, Verdier M, Lu YC, Kung H, Mitchell TE, Nastasi M, et al. *Scr Mater* 1998;39:555.
- [71] Spaepen F, Yu DYW. *Scr Mater* 2003;50:729.
- [72] Tan XH, Shen Y-L. *Compos Sci Technol* 2005;65:1639–46.
- [73] Shen Y-L, Guo YL. *Modell Simul Mater Sci Eng* 2001;9:391–8.
- [74] Kozola BD, Shen YL. *J Mater Sci* 2003;38:901–7.
- [75] Shen Y-L, Williams JJ, Piotrowski G, Chawla N, Guo YL. *Acta Mater* 2001;49:3219–29.
- [76] Pereyra R, Shen Y-L. *Mater Charact* 2004;53:373–80.
- [77] Ege ES, Shen Y-L. *Mater Res Soc Symp Proc* 2003;750:U6.2.
- [78] Durst K, Goken M, Vehoff H. *J Mater Res* 2004;19:85–93.
- [79] Olivas ER, Swadener JG, Shen Y-L. *Scr Mater* 2006;54:263–8.
- [80] Swadener JG, Taljat B, Pharr GM. *J Mater Res* 2001;16:2091.
- [81] Jitcharoen J, Padtare NP, Giannakopoulos AE, Suresh S. *J Am Ceram Soc* 1998;81(9):2301–8.
- [82] Jorgensen O, Giannakopoulos AE, Suresh S. *Int J Solid Struct* 1998;35(36):5097–113.
- [83] Suresh S, Olsson M, Giannakopoulos AE, Padtare NP, Jitcharoen J. *Acta Mater* 1999;47(14):3915–26.
- [84] Pender DC, Padtare NP, Giannakopoulos AE, Suresh S. *Acta Mater* 2001;49(16):3255–62.
- [85] Pender DC, Padtare NP, Giannakopoulos AE, Suresh S. *Acta Mater* 2001;49(16):3263–8.
- [86] Suresh S. *Science* 2001;292(5526):2447–51.
- [87] Thompson SC, Pandit A, Padtare NP, Suresh S. *J Am Ceram Soc* 2002;85(8):2059–64.
- [88] Sampath S, McCune R (Eds). *MRS Bulletin*, July 2000.
- [89] Ma Q, Clarke DR. *J Mater Res* 1995;10(4):853–63.
- [90] Nix WD, Gao H. *J Mech Phys Solids* 1998;46(3):411–25.
- [91] Gane M, Cox JM. *Philos Mag* 1970;22(179):881–91.
- [92] Stelmashenko NA, Walls MG, Brown LM, Milman YV. *Acta Metall Mater* 1993;41(1):2855–65.
- [93] Tymiak NI, Kramer DE, Bahr DF, Gerberich WW. *Acta Mater* 2001;49:1021–34.
- [94] Bahr DF, Kramer DE, Gerberich WW. *Acta Mater* 1998;46(10):3605–17.
- [95] Gao H, Huang Y, Nix WD, Hutchinson JW. *J Mech Phys Solids* 1999;47:1239–63.
- [96] Begley MR, Hutchinson JW. *J Mech Phys Solids* 1998;46:2049–68.
- [97] Shu JY, Fleck NA. *Int J Solid Struct* 1998;35(13):1363–83.
- [98] Hutchinson JW. *Int J Solid Struct* 2000;37:225–38.
- [99] Schwaiger R, Moser B, Dao M, Chollacoop N, Suresh S. *Acta Mater* 2003;51:5159.
- [100] Lu L, Schwaiger R, Shan ZW, Dao M, Lu K, Suresh S. *Acta Mater* 2005;53(7):2169–79.
- [101] Dao et al. *Acta Mater*, in press.
- [102] Gouldstone A, Koh H-J, Zeng K-Y, Giannakopoulos AE, Suresh S. *Acta Mater* 2000;48:2277.
- [103] Page TF, Oliver WC, McHargue CJ. *J Mater Res* 1992;7:450.
- [104] Gerberich WW, Nelson JC, Lilleodden ET, Anderson P, Wyrobek PJT. *Acta Mater* 1996;44:3585.
- [105] Bahr DF, Vasquez G. *J Mater Res* 2005;20:1947.
- [106] Suresh S, Nieh TG, Choi BW. *Scr Mater* 1999;41(9):951.
- [107] Gerberich WW, Kramer DE, Tymiak NI, Volinsky AA, Bahr DF, Kriese MD. *Acta Mater* 1999;47:4115.
- [108] Gerberich WW, Mook WM, Chambers MD, Cordill MJ, Perrey CR, Carter CB, et al. *J Appl Mech* 2006;73:327–34.
- [109] Gerberich WW, Cordill MJ, Mook WM, Moody NR, Perrey CR, Carter CB, et al. *Acta Mater* 2005;53:2215–29.
- [110] Corcoran SG, Colton RJ, Lilleodden ET, Gerberich WW. *Phys Rev B* 1997;55:16057–60.
- [111] Gerberich WW, Venkataraman SK, Huang H, Harvey SE, Kohlstedt DL. *Acta Metall Mater* 1995;43:1569–76.
- [112] Lilleodden ET, Nix WD. *Acta Mater* 2006;54:1583–93.
- [113] Goken M, Sakidja R, Nix WD, Perepezko JH. *Mater Sci Eng A* 2001;319:902–8.
- [114] Asif SAS, Pethica JB. *Philos Mag A* 1997;76:1105–18.
- [115] Gaillard Y, Tromas C, Woigard J. *Philos Mag Lett* 2000;76:2214–6.
- [116] Kucheyev SO, Bradby JE, Williams JS, Jagadish C, Swain MV. *Appl Phys Lett* 2002;80:956–8.
- [117] Mann AB, Pethica JB. *Langmuir* 1996;12:4583–6.
- [118] Woigard J, Tromas C, Girard JC, Audurier V. *J Eur Ceram Soc* 1998;18:2297–305.
- [119] Bhagavat S, Kao I. *Mater Sci Eng A* 2005;393(1–2):327–31.
- [120] Coratolo AM, Orlovskaya N, Lugovy M, Slyunyayev V, Dub S, Johnson C, et al. *J Mater Sci* 2006;41:3105–11.
- [121] Schuh CA. *Mater Today* 2006;9(5):32–9.
- [122] Gerberich WW, Mook WM, Perrey CR, Carter CB, Baskes MI, Mukherjee R, et al. *J Mech Phys Solids* 2003;51:979–92.
- [123] Gerberich WW, Mook WM, Cordill MJ, Carter CB, Perrey CR, Heberlein JV, et al. *Int J Plasticity* 2005;21:2391–405.
- [124] Schaefer DM, Patil A, Andres RP, Reifengerger R. *Phys Rev B* 1995;51:5322–32.
- [125] Greer JR, Oliver WC, Nix WD. *Acta Mater* 2005;53:1821–30.
- [126] Greer JR, Nix WD. *Appl Phys A – Mater Sci Proc* 2005;80:1625–9.
- [127] Greer JR, Nix WD. *Phys Rev B* 2006;73:245410.
- [128] Uchic MD, Dimiduk DM, Florando JN, Nix WD. *Science* 2004;305:986–9.
- [129] Li J, Ngan AHW, Gumbsch P. *Acta Mater* 2003;51:5711–42.
- [130] Elber R, Karplus M. *Chem Phys Lett* 1987;139:375–80.
- [131] Henkelman G, Jonsson H. *J Chem Phys* 2000;113:9978–85.
- [132] Henkelman G, Uberuaga BP, Jonsson H. *J Chem Phys* 2000;113:9901–4.
- [133] Bolhuis PG, Chandler D, Dellago C, Geissler PL. *Ann Rev Phys Chem* 2002;53:291–318.
- [134] Zhu T, Li J, Lin X, Yip S. *J Mech Phys Solids* 2005;53:1597–623.
- [135] Zhu T, Li J, Yip S. *Phys Rev Lett* 2004;93:025503.
- [136] Voter AF, Montalenti F, Germann TC. *Ann Rev Mater Res* 2002;32:321–46.
- [137] Li J, Liao DY, Yip S, Najafabadi R, Ecker L. *J Appl Phys* 2003;93:9072–85.
- [138] Kresse G, Hafner J. *Phys Rev B* 1993;47:558–61.
- [139] Landman U, Luedtke WD, Burnham NA, Colton RJ. *Science* 1990;248:454–61.
- [140] Hoover WG, Degroot AJ, Hoover CG, Stowers IF, Kawai T, Holian BL, et al. *Phys Rev A* 1990;42:5844–53.
- [141] Harrison JA, White CT, Colton RJ, Brenner DW. *Surf Sci* 1992;271:57–67.
- [142] Belak J, Boercker DB, Stowers IF. *MRS Bull* 1993;18:55–60.
- [143] Kallman JS, Hoover WG, Hoover CG, Degroot AJ, Lee SM, Womton F. *Phys Rev B* 1993;47:7705–9.
- [144] Komvopoulos K, Yan W. *J Appl Phys* 1997;82:4823–30.
- [145] Sinnott SB, Colton RJ, White CT, Shenderova OA, Brenner DW, Harrison JA. *J Vac Sci Tech A* 1997;15:936–40.

- [146] Kelchner CL, Plimpton SJ, Hamilton JC. *Phys Rev B* 1998;58:11085–8.
- [147] Tadmor EB, Miller R, Phillips R, Ortiz M. *J Mater Res* 1999;14:2233–50.
- [148] Picu RC. *J. Comput. – Aided Mater. Des.* 2000;7:77–87.
- [149] Shenoy VB, Phillips R, Tadmor EB. *J Mech Phys Solids* 2000;48:649–73.
- [150] Walsh P, Kalia RK, Nakano A, Vashishta P, Saini S. *Appl Phys Lett* 2000;77:4332–4.
- [151] Gannepalli A, Mallapragada SK. *Nanotechnology* 2001;12:250–7.
- [152] Zimmerman JA, Kelchner CL, Klein PA, Hamilton JC, Foiles SM. *Phys Rev Lett* 2001;87:16:165507.
- [153] de la Fuente OR, Zimmerman JA, Gonzalez MA, de la Figuera J, Hamilton JC, Pai WW, et al. *Phys Rev Lett* 2002;88:036101.
- [154] Li J, Van Vliet KJ, Zhu T, Yip S, Suresh S. *Nature* 2002;418:307–10.
- [155] Feichtinger D, Derlet PM, Van Swygenhoven H. *Phys Rev B* 2003;67:024113.
- [156] Knap J, Ortiz M. *Phys Rev Lett* 2003;90:226102.
- [157] Liang HY, Woo CH, Huang HC, Ngan AHW, Yu TX. *Philos Mag* 2003;83:3609–22.
- [158] Lilleodden ET, Zimmerman JA, Foiles SM, Nix WD. *J Mech Phys Solids* 2003;51:901–20.
- [159] Ma XL, Yang W. *Nanotechnology* 2003;14:1208–15.
- [160] Smith R, Christopher D, Kenny SD, Richter A, Wolf B. *Phys Rev B* 2003;67:245405.
- [161] Van Vliet KJ, Li J, Zhu T, Yip S, Suresh S. *Phys Rev B* 2003;67:104105.
- [162] Walsh P, Omeltchenko A, Kalia RK, Nakano A, Vashishta P, Saini S. *Appl Phys Lett* 2003;82:118–20.
- [163] Cha PR, Srolovitz DJ, Vanderlick TK. *Acta Mater* 2004;52:3983–96.
- [164] Hasnaoui A, Derlet PM, Van Swygenhoven H. *Acta Mater* 2004;52:2251–8.
- [165] Jeng YR, Tan CM. *Phys Rev B* 2004;69:104109.
- [166] Miller RE, Shilkrot LE, Curtin WA. *Acta Mater* 2004;52:271–84.
- [167] Sanz-Navarro CF, Kenny SD, Smith R. *Nanotechnology* 2004;15:692–7.
- [168] Schall JD, Brenner DW. *J Mater Res* 2004;19:3172–80.
- [169] Szlufarska I, Kalia RK, Nakano A, Vashishta P. *Appl Phys Lett* 2004;85:378–80.
- [170] Lee YM, Park JY, Kim SY, Jun S, Im S. *Mech Mater* 2005;37:1035–48.
- [171] Saraev D, Miller RE. *Modell Simul Mater Sci Eng* 2005;13:1089–99.
- [172] Shi YF, Falk ML. *Appl Phys Lett* 2005;86:011914.
- [173] Shiari B, Miller RE, Curtin WA. *J Eng Mater Technol* 2005;127:358–68.
- [174] Szlufarska I, Kalia RK, Nakano A, Vashishta P. *Phys Rev B* 2005;71:174113.
- [175] Szlufarska I, Kalia RK, Nakano A, Vashishta P. *Appl Phys Lett* 2005;86:021915.
- [176] Szlufarska I, Nakano A, Vashishta P. *Science* 2005;309:911–4.
- [177] Hagelaar JHA, Bitzek E, Flipse CFJ, Gumbsch P. *Phys Rev B* 2006;73:045425.
- [178] Perez R, Payne MC, Simpson AD. *Phys Rev Lett* 1995;75:4748–51.
- [179] Smith GS, Tadmor EB, Kaxiras E. *Phys Rev Lett* 2000;84:1260–3.
- [180] Smith GS, Tadmor EB, Bernstein N, Kaxiras E. *Acta Mater* 2001;49:4089–101.
- [181] Fago M, Hayes RL, Carter EA, Ortiz M. *Phys Rev B* 2004;70:100102.
- [182] Hayes RL, Fago M, Ortiz M, Carter EA. *Multiscale Model Simul* 2005;4:359–89.
- [183] Holian BL, Voter AF, Wagner NJ, Ravelo RJ, Chen SP, Hoover WG, et al. *Phys Rev A* 1991;43:2655–61.
- [184] Harrison JA, White CT, Colton RJ, Brenner DW. *Phys Rev B* 1992;46:9700–8.
- [185] Garg A, Sinnott SB. *Phys Rev B* 1999;60:13786–91.
- [186] Brenner DW, Shenderova OA, Harrison JA, Stuart SJ, Ni B, Sinnott SB. *J Phys – Condens Matter* 2002;14:783–802.
- [187] Schall P, Cohen I, Weitz DA, Spaepen F. *Nature* 2006;440:319–23.
- [188] Gouldstone A, Van Vliet KJ, Suresh S. *Nature* 2001;411:656.
- [189] Li J, Yip S. *CMES – Comp Model Eng Sci* 2002;3:219–27.
- [190] Ogata S, Li J, Yip S. *Science* 2002;298:807–11.
- [191] Ogata S, Li J, Hirosaki N, Shibutani Y, Yip S. *Phys Rev B* 2004;70:104104.
- [192] Clatterbuck DM, Krenn CR, Cohen ML, Morris JW. *Phys Rev Lett* 2003;91:135501.
- [193] Van Vliet KJ, Tsikata S, Suresh S. *Appl Phys Lett* 2003;83:1441–3.
- [194] Yoon JH, Kim SJ, Jang H. *Prop Adv Eng Mater* 2004;449–454(1–2):89–92.
- [195] Wang Y, Raabe D, Kluber C, Roters F. *Acta Mater* 2004;52:2229–38.
- [196] Broughton JQ, Abraham FF, Bernstein N, Kaxiras E. *Phys Rev B* 1999;60:2391–403.
- [197] Patzold G, Linke A, Hapke T, Heermann DW. *Z Phys B* 1997;104:513–21.
- [198] Ferrando R, Andrei M, Relini A, Rolandi R, Gliozzi A. *Phys Rev B* 2005;72:045412.
- [199] Thalladi VR, Schwartz A, Phend JN, Hutchinson JW, Whitesides GM. *J Am Chem Soc* 2002;124:9912–7.
- [200] Mukherjee S, Murray S, Khraishi T, Shen Y-L. *Mol Simul* 2006;32:339–43.
- [201] Robertson CF, Fivel MC. *J Mater Res* 1999;14:2251–8.
- [202] Fivel MC, Robertson CF, Canova GR, Boulanger L. *Acta Mater* 1998;46:6183–94.
- [203] Mishin Y, Mehl MJ, Papaconstantopoulos DA, Voter AF, Kress JD. *Phys Rev B* 2001;63:22:224106.
- [204] Zhu T, Li J, Van Vliet KJ, Ogata S, Yip S, Suresh S. *J Mech Phys Solids* 2004;52:691–724.
- [205] Tadmor EB, Ortiz M, Phillips R. *Philos Mag A* 1996;73:1529–63.
- [206] Shilkrot LE, Miller RE, Curtin WA. *J Mech Phys Solids* 2004;52:755–87.
- [207] Widjaja A, Van der Giessen E, Needleman A. *Mater Sci Eng A* 2005;400:456–9.
- [208] Arsenlis A, Parks DM, Becker R, Bulatov VV. *J Mech Phys Solids* 2004;52:1213–46.
- [209] Dmitriev SV, Kitamura T, Li J, Umeno Y, Yashiro K, Yoshikawa N. *Acta Mater* 2005;53:1215–24.
- [210] Li J, Zhu T, Yip S, Van Vliet KJ, Suresh S. *Mater Sci Eng A* 2004;365:25–30.
- [211] Hill R. *J Mech Phys Solids* 1962;10:1–16.
- [212] Leroy Y, Ortiz M. *Int J Numer Anal Methods Geomech* 1989;13:53–74.
- [213] Zhu T, Li J, Yip S. *Phys Rev Lett* 2004;93:205504.
- [214] Wo PC, Zuo L, Ngan AHW. *J Mater Res* 2005;20:489–95.
- [215] Mason JK, Lund AC, Schuh CA. *Phys Rev B* 2006;73:054102.
- [216] Vineyard GH. *J Phys Chem Solids* 1957;3:121–7.
- [217] Kocks UF, Argon AS, Ashby MF. *Mater Sci* 1975;19:1–281.
- [218] Schuh CA, Mason JK, Lund AC. *Nat Mater* 2005;4:199.
- [219] Henkelman G, Jonsson H. *J Chem Phys* 1999;111:7010–22.
- [220] Elber R. *Curr Opin Struct Biol* 2005;15:151–6.
- [221] Bulatov VV, Yip S, Argon AS. *Philos Mag A* 1995;72:453–96.
- [222] Rasmussen T, Jacobsen KW, Leffers T, Pedersen OB, Srinivasan SG, Jonsson H. *Phys Rev Lett* 1997;79:3676–9.
- [223] Rasmussen T, Vegge T, Leffers T, Pedersen OB, Jacobsen KW. *Philos Mag A* 2000;80:1273–90.
- [224] Vegge T, Rasmussen T, Leffers T, Pedersen OB, Jacobsen KW. *Phys Rev Lett* 2000;85:3866–9.
- [225] Vegge T, Jacobsen W. *J Phys – Condens Matter* 2002;14:2929–56.
- [226] Fang TH, Weng CI, Chang JG. *Mater Sci Eng A* 2003;357:7–12.
- [227] Zhu T, Li J, Yip S. *Proc R Soc London A* 2006;462:1741–61.
- [228] Domnich V, Gogotsi Y, Dub S. *Appl Phys Lett* 2000;76:2214–6.
- [229] Bradby JE, Williams JS, Swain MV. *Phys Rev B* 2003;67:085205.
- [230] Minor AM, Lilleodden ET, Jin M, Stach EA, Chrzan DC, Morris Jr JW. *Philos Mag* 2005;85(2–3):323–30.
- [231] Ohmura T, Minor AM, Stach EA, Morris Jr JW. *J Mater Res* 2004;19(12):3626–32.
- [232] Minor AM, Morris Jr JW, Stach EA. *Appl Phys Lett* 2001;79:1625.

- [233] Jin M, Minor AM, Stach EA, Morris Jr JW. *Acta Mater* 2004;52:5381–7.
- [234] Minor AM, Stach EA, Morris Jr JW, Petrov I. *J Elect Mater* 2003;32(10):1023–7.
- [235] Minor AM, Lilleodden ET, Stach EA, Morris Jr JW. *J Mater Res* 2004;19:176–82.
- [236] Alexander H, Haasen P. *Solid State Phys* 1968;22:27.
- [237] Sumino K. In: Moss TS, Mahajan S, editors. *Handbook on semiconductors, materials, properties and preparation*, vol. 3A. Amsterdam: Elsevier; 1994. p. 73.
- [238] Lawn BR. *Fracture of brittle solids*. Cambridge: Cambridge University Press; 1993.
- [239] Hill MJ, Rowcliffe DJ. *J Mater Sci* 1974;9:1569.
- [240] Pharr GM, Oliver WC, Harding DS. *J Mater Res* 1991;6:1129.
- [241] Mann AB, van Heerden D, Pethica JB, Weihs TP. *J Mater Res* 2000;15:1754–8.
- [242] Weppelmann ER, Field JS, Swain MV. *J Mater Res* 1993;8:830.
- [243] Saka H, Shimatani A, Sukanuma M, Suprijadi M. *Philos Mag A* 2002;82:1971.
- [244] Minor AM, Lilleodden ET, Jin M, Stach EA, Chrzan DC, Morris Jr JW. *Philos Mag* 2005;85:323–30.
- [245] Hirsch P, Howie A, Nicholson RB, Pashley DW, Whelan MJ. *Electron microscopy of thin crystals*. Malabar, FL: Krieger; 1977.
- [246] Bradby JE, Williams JS, Wong-Leung J, Swain MV, Munroe P. *Appl Phys Lett* 2000;77:3749.
- [247] Clarke DR, Kroll MC, Kirchner PD, Cook RF, Hockey BJ. *Phys Rev Lett* 1988;60:2156.
- [248] Perez R, Payne MC, Simpson AD. *Phys Rev Lett* 1995;75:4748.
- [249] Hall EO. *Proc Phys Soc London* 1951;B64:747.
- [250] Petch NJ. *J Iron Steel Inst* 1953;174:25.
- [251] Li JCM. *Trans Metall Soc AIME* 1963;227:239.
- [252] Langdon T. *Mater Sci Eng A* 1992;137:1–11.
- [253] Langdon T. *Met Trans A* 1982;B13A:689–700.
- [254] Winning M, Gottstein G, Shvindlerman LS. *Acta Mater* 2001;49:211–9.
- [255] Merkle KL, Thompson LJ. *Mater Lett* 2001;48:188–93.
- [256] Soer WA, De Hosson JThM, Minor AM, Morris Jr JW, Stach EA. *Acta Mater* 2004;52:5783–90.
- [257] Minor AM, Lilleodden ET, Stach EA, Morris Jr JW. *J Elect Mater* 2002;31:958.
- [258] This is research was supported in part by a US Department of Energy SBIR grant (DE-FG02-04ER83979) awarded to Hysitron, Inc. which does not constitute an endorsement by DOE of the views expressed in the article.
- [259] Minor AM, Syed Asif SA, Shan ZW, Stach EA, Cyranowski E, Wyrobek TJ, et al. *Nat Mater* 2006;5:697–702.
- [260] Soer WA, De Hosson JThM, Minor AM, Shan Z, Syed Asif SA, Warren OL. submitted for publication.
- [261] Warren OL, Syed Asif SA, Stach EA, Minor AM, in preparation.
- [262] Shan Z, Cabot A, Minor AM, Syed Asif SA, Warren OL, Chrzan DC, Alivisatos AP, in preparation.
- [263] Saito R, Dresselhaus MS, Dresselhaus G. *Physical properties of carbon nanotubes*. London: Imperial College Press; 2006.
- [264] Ebbesen TW, Ajayan PM. *Nature* 1992;358:220–2.
- [265] Treacy MMJ, Ebbesen TW, Gibson JM. *Nature* 2002;381:678–80.
- [266] Wong EW, Sheehan PE, Lieber CM. *Science* 1997;277:1971–5.
- [267] Salveta JP, Bonard JM, Thomson NH, Kulik AJ, Forro L, Benoit W, et al. *Appl Phys A* 1999;69:255–60.
- [268] Cao AY, Dickrell PL, Sawyer WG, Ghasemi-Nejhad MN, Ajayan PM. *Science* 2005;310(5752):1307–10.
- [269] Qi HJ, Teo KBK, Lau KKS, Boyce MC, Milne WI, Robertson J, et al. *J Mech Phys Solids* 2003;51(11–12):2213–37.
- [270] Pantano A, Boyce MC, Parks DM. *J Mech Phys Solids* 2004;52(4):789–821.
- [271] Cao GX, Chen X. *Phys Rev B*. *Phys Rev B* 2006;73(15). Art No 155435.
- [272] Dickrell PL, Sinnott SB, Hahn DW, Raravikar NR, Schadler LS, Ajayan PM, et al. *Tribol Lett* 2005;18(1):59–62.
- [273] Liu C, Cheng HM, Cong HT, Li F, Su G, Zhou BL, et al. *Adv Mater* 2000;12(16):1190–2.
- [274] Iannotta B. *Aerospace Am* 2006;44(3):30–5.
- [275] Barbakadze N, Enders S, Gorb S, Arzt E. *J Exptl Bio* 2006;209:722–30.
- [276] Lichtenegger HC, Schoberl T, Bartl MH, Waite H, Stucky GD. *Science* 2002;298:389–92.
- [277] Lewis G, Xu J, Dunne N, Daly C, Orr J. *J Biomed Mater Res B* 2006;78B:312–7.
- [278] Donnelly E, Baker SP, Boskey AL, van der Meulen MCH. *J Biomed Mater Res A* 2006;77A:426–35.
- [279] Hajji MA, Wilson TA, Lai-Fook SJ. *J Appl Physiol* 1979;47:175–81.
- [280] Gouldstone A, Brown RE, Butler JP, Loring SH. *J Appl Physiol* 2003;95(6):2345–9.
- [281] Brismar B, Hedenstierna G, Lundquist H, Strandberg A, Svensson L, Tokics L. *Anesthesiology* 1985;62(4):422–8.
- [282] Magnusson L, Spahn DR. *Br J Anaesthesia* 2003;91(1):61–72.
- [283] Wellman PS, Dalton EP, Krag D, Kern KA, Howe RD. *Arch Surg* 2001;136(2):204–8.
- [284] Wang BC, Wang GR, Yan DH, Liu YP. *Biomed Mater Eng* 1992;2(3):133–8.
- [285] Kerdok AE, Cotin SM, Ottensmeyer MP, Galea AM, Howe RD, Dawson SL. *Med Image Anal* 2003;7(3):283–91.
- [286] Szekely G, Brechbuhler C, Dual J, Enzler R, Hug J, Hutter R, et al. *Presence – Teleoperat Virt Environ* 2000;9(3):310–33.
- [287] Dandekar K, Raju BA, Srinivasan MA. *J Biomech Eng* 2003;125:682–91.
- [288] Kao I, Yang FQ. *IEEE Trans Robot Automat* 2004;20(1):132–5.
- [289] Bhagavat S, Kao I. *Int J Mach Tools Manuf* 2006;46(5):531–41.
- [290] Luo JF, Dornfeld DA. *IEEE Trans Semiconductor Manuf* 2001;14(2):112–33.
- [291] Bifano TG, Dow TA, Scattergood RO. *J Eng Industry – Trans ASME* 1991;113(2):184–9.
- [292] Puttick KE, Whitmore LC, Zhdan P, Gee AE, Chao CL. *Tribol Int* 1995;28(6):349–55.
- [293] Uddin MS, Seah KHW, Li XP, Rahman M, Liu K. *Wear* 2004;257(7–8):751–9.
- [294] Blake PN. *J Am Ceram Soc* 1990;73:949.
- [295] Patten J, Gao WI, Yasuto K. *J Manuf Sci Eng* 2005;127:522–32.
- [296] Morris JC. *J Am Ceram Soc* 1995;78:2015.
- [297] Gogotsi YG. *Mater Res Innov* 1997;1:3.
- [298] Yan JW, Takahashi H, Tamaki J, Gai XH, Harada H, Patten J. *Appl Phys Lett* 2005;86:181913.
- [299] Gilman JJ. *Philos Mag B* 1993;67:207.
- [300] Pizani PS, Jasinevicius RG, Zanatta AR. *Appl Phys Lett* 2006;89:031917.
- [301] Pharr GM, Oliver WC, Clarke DR. *Scripta Met* 1989;23:1949–52.
- [302] Juliano T, Gogotsi Y, Dominich V. *J Mater Res* 2003;18:1192–201.
- [303] Chou SY, Krauss PR, Renstrom PJ. *Appl Phys Lett* 1995;67(21):3114–6.
- [304] Le NV, Dauksher WJ, Gehoski KA, Nordquist KJ, Ainley E, Mangat P. *Microelectron Eng* 2006;83(4–9):839–42.
- [305] He JH, Hsu JH, Wang CW, Lin HN, Chen LJ, Wang ZL. *J Phys Chem B* 2006;110(1):50–3.
- [306] Tweedie CA, Anderson DG, Langer R, Van Vliet KJ. *Adv Mater* 2005;17:2599–604.
- [307] Han SM, Shah R, Banerjee R, Viswanathan GB, Clemens BM, Nix WD. *Acta Mater* 2005;53:2059–67.